ERASMUS UNIVERSITY ROTTERDAM

Erasmus School of Economics

Bachelor Thesis Econometrics and Operations Research

Predictability in Scale-specific Systems

Name student: Thomas Kornelis Gijsbert Brink

Student ID number: 455893

Supervisor: Grith, M.

Second assessor: Wit, K.P. de

Date final version: 7 July 2019

Abstract

This paper investigates the hump-shaped behavior of slopes and coefficients of determination of predictive regressions for future excess market returns on past regressors, as discussed by Bandi, Perron, Tamoni, and Tebaldi (2019). In doing so, the results of the former paper for two-way aggregated regression models and classical predictive systems are first reviewed, after which the scale-specific framework proposed by Bandi et al. (2019) is extended threefold. Firstly, a robustness analysis is conducted to investigate the sensitivity of presented results to slight model changes. Secondly, a high-frequency analysis is employed. Thirdly, this research formally addresses the idea of incorporating multiple regressors in scale-wise predictive systems. This paper finds that hump-shaped behavior and scale-specific predictability remain to hold under altered data and sample adjustments, while the location of predictability peaks may vary over scales. High-frequency data supports the findings of Bandi et al. (2019) for the NYSE/AMEX and S&P 500 indices, while the occurrence of hump-shaped behavior in other markets is not definitive. Adding multiple regressors preserves hump-shaped behavior, while predictability reaches up to 90%.

Keywords: *Risk-return tradeoff*; *Aggregation*; *Hump-shaped behavior*; *Scale*; *Predictability*; *Robustness*; *Frequency*; *Multivariate regression*

Table of Contents

1 Introduction **3**

2 Literature Review **4**

3 Data **7**

4 Methodology **8**

4.1 Replication 8

4.1.1 Aggregated Regressions 8

4.1.2 Scale-specific framework 9

4.2 Extension 12

4.2.1 Robustness Analysis 12

4.2.2 High-frequency Analysis 12

4.2.3 Multiple Regressor System 13

5 Results **14**

5.1 Replication 14

5.1.1 Aggregated Regressions 14

5.1.2 Scale-specific Framework 15

5.2 Extension 18

5.2.1 Robustness Analysis 18

5.2.2 High-frequency Analysis 19

5.2.3 Multiple Regressor System 21

6 Conclusion & Discussion **21**

7 Acknowledgements **22**

A Excess Market Returns Data **26**

B Classical Predictive System Aggregation **29**

C Dyadic Scales **30**

D Haar transformation **31**

E Aggregated Regression Tables **32**

F Simulation A **33**

F.1 Predictability 33

F.2 No predictability 35

G Multiple Regressor System **37**

H Simulation B **38**

H.1 Predictability 38

H.2 No predictability 39

H.3 Contemporaneous Aggregation 40

I Note **42**

J Monthly returns derivation **43**

K Codes **44**

K.1 Folder Annual Analysis 44

K.2 Folder High-frequency Extension 45

K.3 Folder Simulations 45

K.4 Folder Exact Replication Codes 45

1 Introduction

In the field of finance, predicting returns is one of the most relevant issues. Previous research has drawn a wide variety of conclusions, both in favor of (Cochrane, 2007) and against (Welch & Goyal, 2007) the notion of predictability. Furthermore, a wide variety of predictors and approaches have been implemented, see for instance Lewellen (2004) for a discussion. This research draws on one of the main issues recurring in research on explaining and forecasting returns, namely the low signal-to-noise problem (Torous & Valkanov, 2000).

As in Bandi and Perron (2008), this paper aims to tackle the above problem by looking into long-run movements of returns, as explained by variance. Through forward/backward aggregation of returns and variance, the signal is strengthened relative to the reduced noise. Bandi et al. (2019) build on the aggregated model by investigating the predictive relationship between returns and variance over an aggregation horizon of up to 20 years. They find that this relationship exhibits so-called 'hump-shaped' behavior, with a predictive peak occurring at a horizon of around 16 years. Furthermore, classical predictive systems are shown to be unable to replicate such behavior.

To find a data generating process capable of displaying the aggregated return-variance relationship, Bandi et al. (2019) propose a modelling framework in which time series are decomposed in components bearing different scales or frequencies of cyclical movements, resembling that of Ortu, Severino, Tamoni, and Tebaldi (2017). Evaluation of the predictability in separated scale-specific components leads, upon two-way aggregation, to a peak around 16 years being once again found.

The research by Bandi et al. (2019) thus not only uncovers predictability of returns in the long run, but also introduces a scale-specific model capturing the long-run dynamics well. This paper aims to further increase this relevance by providing three extensions on the work by Bandi et al. (2019), after first reviewing the corresponding results. From replicating, this research concludes that small discrepancies in results arise due to ambiguities in data processing. However, these discrepancies do not affect the hump-shaped behavior nor the notion of scale-specific predictability.

As for the first extension, I perform a robustness analysis to check the sensitivity of the scale-specific framework to slight modelling changes. These encompass i) a shift in the market index, ii) sample period adjustments, and iii) varying frequencies between returns and variance simultaneously. I show that a change from the NYSE/AMEX to the S&P 500 does not affect results to any notable extent. In correspondence with Campbell (1991), I change the sample to the post-war period, for which the notion of hump-shaped behavior does not change. However, the location and magnitude

of predictive peaks are shown to be substantially affected. Finally, this paper confirms the remark of Bandi and Perron (2008), stating that equality in aggregation horizons for returns and variance does not necessarily yield maximal predictability, although being relatively close to 'optimal'.

Secondly, this research extends the work of Bandi et al. (2019) by performing high-frequency analysis, i.e. taking monthly instead of yearly observations as its basis. Due to this basis, the grouping of scales has preferable properties concerning predictive peaks, in addition to the advantage that the number of data points increases. Hump-shaped behavior and scale-specific predictability for the NYSE/AMEX and S&P 500 index are convincingly supported, while an analysis of the British and Dutch stock market, via the FTSE 100 and AEX, does not lead to clear conclusions.

Finally, this paper introduces multiple predictors, including the dividend yield and inflation, besides variance in the scale-specific framework. The inclusion of these predictors allows long-run predictability to reach up to 90%, implying an apparent use and relevance of using multiple regressors.

This paper will continue with a detailed literature review, after which the data for this research are briefly described. Consequently, Section 4 summarizes the framework of Bandi et al. (2019) and provides the basis for this research's extensions. Subsequently, the findings from reviewing Bandi et al. (2019) are presented, after which the extension results follow. Finally, this paper concludes and provides discussion points as well as possibilities for future research.

2 Literature Review

In the field of finance, the relationship between risk and returns is a widely reviewed topic. French, Schwert, and Stambaugh (1987) state that there is a positive relationship between expected risk premia and predictable volatility, while Nelson (1991) argues the opposite is true. As Lundblad (2007) identify, such statements are heavily dependent on the sample size, finding a positive risk-return tradeoff in the long run. Although the above research constitutes linking expected excess returns to *future* volatility, the interest of this paper is to link return predictability to *past* variance.

By performing predictive regressions of stock returns on risk measures, Goyal and Santa-Clara (2003) find that such predictability is not or hardly present over the short term. More generally speaking, predictability of returns over the short term suffers from the so-called signal-to-noise problem (Torous & Valkanov, 2000). Due to the relatively large noise in predictive regressions, true informative signals may be hidden behind shocks. Valkanov (2003) argues that, by construction, the signal is amplified in the long run, whereas the effect of shocks diminishes so that aggregations

of return horizons can lead to uncovering predictability (Fama & French, 1988) .

Similarly, Bandi and Perron (2008) investigate the long-run predictability of forward aggregated excess market returns by backward aggregated market variance. An increased dependence and explanatory power is found with an increasing horizon, where horizons up to 10 years are considered. Bandi et al. (2019) generalize forward-backward regressions for aggregation horizons up to 20 years. These regressions are performed on three different variance proxies, the first of which being realized market variance (Andersen, Bollerslev, Diebold, & Labys, 2001). Secondly, consumption variance is employed, based on Tamoni (2011), while the third measure relates to economic policy uncertainty, to be named *EPU* henceforth (Baker, Bloom, & Davis, 2016).

For all three measures, hump-shaped behavior is found; the slopes and coefficients of determination of regressions increase until reaching a certain peak, after which a decrease kicks in. A predictive peak is found at a horizon of around 16 years, where the R^2 reaches about 55%. Contrastingly, classical predictive systems, based on modelling variance as an autoregressive process of order 1, are shown to be unable to yield similar behavior (Bandi & Perron, 2008). Therefore, Bandi et al. (2019) propose a new modelling framework.

The idea behind this framework lies in scale-specific modelling; separating series in *components* with various frequencies. The decomposition of time series into transitory and persistent components is introduced by Beveridge and Nelson (1981), after which a substantial amount of literature has followed, e.g. Bollerslev, Osterrieder, Sizova, and Tauchen (2013), Daniel and Torous (1991) and Lee and Engle (1993). A common application has been measuring business cycles (Baxter & King, 1999), for which oscillations with a frequency over 8 years are usually incorporated in the trend or persistent component, see Zarnowitz and Ozyildirim (2006) and Yogo (2008). Contrastingly, Bandi et al. (2019) consider transitory components with frequencies over 8 years, which may be of significant importance (Comin & Gertler, 2006). Besides frequencies, modelling and identification of regular time series to components usually vary across papers. The approach Bandi et al. (2019) take, is that of modelling through (extended) Wold representations and identification via multiresolution filters. The decomposition formally follows from Ortu et al. (2017) and Ortu, Tamoni, and Tebaldi (2013), where component-wise observations are contained in so-called decimated observations, i.e. a small number of observations that 'summarize' all informative data (Müller & Watson, 2008).

Based on these decimated points, Bandi et al. (2019) introduce a DGP in which the interdependence between returns and variance is modelled via scale-specific classical predictive systems. In doing so, predictability of returns by uncertainty components can directly be evaluated, which is

dubbed *scale-specific predictability*. A predictive peak is found for cycles between 8 and 16 years, which, due to a one-to-one relationship between decimated observations and aggregated time series, can be translated into hump-shaped behavior in forward/backward aggregated regressions (Bandi et al., 2019). It might be argued that the results presented by Bandi et al. (2019) are extremely volatile to slight changes in the sample, time series or variables. For that reason, this research performs a so-called robustness analysis.

Most research on decomposition of returns and variance makes use of the NYSE/AMEX index, see for instance Bandi and Perron (2008) and Lundblad (2007). However, using a different data set might lead to different results. As in Chen (2009), this research therefore includes a predictability study based on the S&P 500 index. Secondly, it has become common practice consider post-war samples when investigating returns and variances, as volatility and interest structures between pre- and post-war periods differ substantially, see Ding, Granger, and Engle (1993) and Campbell (1991). Therefore, this research investigates the effects of changing the sample to the post-war period. Thirdly, looking into two-way aggregated regressions, it has been common practice to use the same aggregation horizon for both the regressor and regressand (French et al., 1987). On the other hand, Ghysels, Santa-Clara, and Valkanov (2005) and Bandi and Perron (2008) investigate the risk-return tradeoff using different windows for return and variance, where it is found that predictability is not necessarily largest for equal horizons.

The second extension rests on the frequency of sampling. Previous research has consisted of analyses based on both monthly, e.g. Bandi and Perron (2008), and yearly data, e.g. Bandi et al. (2019). Some argue that yearly data is less likely to be influenced by measurement errors (Bansal, Kiku, & Yaron, 2009), whereas others claim that monthly data is more insightful and should be preferred in financial applications Ghysels, Santa-Clara, and Valkanov (2006). The third extension is based on return predictors, for which an enormous amount of literature exists. One of the most commonly researched predictors is the dividend yield, see for instance Cochrane (2007) and Cochrane (2009). This variable has been implemented in both short-run (Ang & Bekaert, 2006) and aggregated models (Fama & French, 1988). Other predictors include financial ratios (Lewellen, 2004), interest rate variables (Fama & French, 1989), inflation (Fama & Schwert, 1977) or other macroeconomic variables such as monetary policy (Patelis, 1997), employment (Asprem, 1989) and (nominal) exchange rates (Chen, 2009). Note that most of the above papers consider return predictability for a single predictor, Bandi and Perron (2008) being a notable exception. The predictability of market variance in aggregated regressions is shown to not or only slightly be affected by the inclusion of

an additional predictor (dividend yield). Instead of considering a bivariate model, this research will look into multivariate (scale-specific) systems.

3 Data

Replication of the research by Bandi et al. (2019) requires data on excess market returns and the three variance proxies (market variance, consumption variance, and economic policy uncertainty). Data on market returns is obtained as monthly value-weighted returns from the NYSE/AMEX index including dividends via the Chicago Center for Research in Security Prices (CRSP). By annualizing and taking the natural logarithm, yearly continuously compounded market returns are obtained. Subtracting the logarithmic forward-looking, end-of-the-year 3-month Treasury Bill rate, obtained via the National Bureau of Economic Research (NBER, 1926 to 1933) and the Federal Reserve Economic Data (1934 to 2018), yields yearly excess returns.

The yearly market variance is obtained as the sum of squared daily returns, now excluding dividends, in a year, of course again taken from the NYSE/AMEX index (CRSP). The consumption variance is readily retrieved from Bandi et al. (2019), while, for the EPU measure, historical data on the economic policy uncertainty index is extracted online[1]. The sample is maximized for all three measures, so that the data set constitutes data from 1926 to 2018 for market variance, 1930 to 2014 for consumption variance, and 1926 to 2014 for EPU.

For the extensions, additional data is used. The robustness analysis requires data from the S&P index, which is similarly retrieved from the CRSP (with the same sample period) as the NYSE/AMEX returns. For the high-frequency analysis, monthly instead of yearly data is used. Still, the data is retrieved from the same sources and in a similar manner. Also, data on the AEX and FTSE 100 is used, with sample periods 1983 to June 2019 and 1984 to June 2019 (source: Datastream). The multiple regressor system requires inflation and dividend yield data for the NYSE/AMEX index. Inflation data are retrieved from the Federal Reserve Bank, while dividend yield data is gathered once again via the CRSP. The sample period considered here matches that of Bandi et al. (2019), namely 1930 to 2014.

In the sense of data transformations for excess market returns, this paper differs slightly from the approach of the authors. I strongly believe that Bandi et al. (2019) make slight mistakes in data processing so that their results are not correct. An extensive argumentation and description of the complete data transformation procedure for returns is attached in Appendix A.

[1] http://www.policyuncertainty.com/

4 Methodology

In this section, I will first discuss replicating the findings presented by Bandi et al. (2019), after which the three separate extensions will be discussed.

4.1 Replication

For the replication part, we will distinguish analysis on aggregated regressions and scale-specific components.

4.1.1 Aggregated Regressions

The first finding presented by Bandi et al. (2019) is that of hump-shaped behavior in the slopes and coefficients of determination when performing aggregated, non-overlapping, regressions of future excess market returns on past variance. Such regressions, conducted over horizon h, can be written as

$$r_{t+1,t+h} = \alpha_h + \beta_h v_{t-h+1,t} + \epsilon_{t+1,t+h} \qquad t = h, ..., T-h \ , \tag{1}$$

where $r_{t+1,t+h} = \sum_{i=t+1}^{t+h} r_i$ is the *h-forward* sum of excess market returns and $v_{t-h+1,t} = \sum_{i=t+1}^{t+h} v_{i-h}$ is the *h-backward* sum of variance (and correspondingly; $\epsilon_{t+1,t+h} = \sum_{i=t+1}^{t+h} \epsilon_i$). In the above equation, $h = 1, ..., H$ denotes the aggregation horizon. Bandi et al. (2019) choose a maximum horizon H of 20 years. In the above, the variance v is taken to be either one of the three measures *market variance*, *consumption variance* or *EPU* (see Section 3).

Investigating the behavior of β_h and the R^2 in (1), Bandi et al. (2019) find that both exhibit hump-shaped behavior over the horizon h, which goes for all three variance proxies. By performing similar forward/backward regressions, I will aim to verify this notion.

Bandi et al. (2019) argue that the hump-shaped pattern can not be achieved by means of classical AR(1) predictive systems, for which returns and variance (both demeaned) are modelled as

$$r_{t+1} = \beta v_t + u_{t+1} \tag{2}$$

$$v_{t+1} = \rho v_t + e_{t+1} \ , \tag{3}$$

When forward aggregating returns and backward aggregating variance via this system, the slope of regression (1) becomes $\beta\rho^{h-1}$ (see Appendix B for the corresponding derivation), which, due to the fact that $|\rho| \leq 1$ by definition (correlation property), does not increase with aggregation horizon h. Therefore, performing two-way aggregated predictive regressions should not yield hump-shaped behavior. Note that Bandi et al. (2019) state that the slope equals $\beta\rho^h$, which thus slightly

deviates from our derivation. To check for hump-shaped behavior, I simulate the data generating processes (2) and (3) for which specifics are provided in Online Supplement A of Bandi et al. (2019)[2]. Forward/backward aggregation of returns and variance consequently lets us investigate the behavior of the regression slopes and coefficients of determination via (1).

4.1.2 Scale-specific framework

In contrast to classical predictive systems, Bandi et al. (2019) argue that, by separating return and variance series into certain scales or frequencies, a data generating process capable of capturing the hump-shaped behavior can be formed. By filtering data into scale-wise *components*, information can be separated into long- and short-term cycles, bearing different informative values. In correspondence with Bandi et al. (2019), this research will be based on cycles with a frequency that increases like powers of 2. Specifically, the $j-th$ component consists of cyclical movements with a frequency between 2^{j-1} and 2^j years. This so-called dyadic property is illustrated in Table 7, see Appendix C. The maximum scale employed will, in the remainder of this paper, be denoted by J.

In the remainder of this section, the decomposition will be explained by using the general notation for a time series x_t. However, the complete decomposition holds for any other (weakly stationary) time series, so that the following process can directly be applied to both returns r_t and variance v_t.

Both Bandi et al. (2019) and Ortu et al. (2013) start by defining the process x_t as

$$x_t = \sum_{j=1}^{+\infty} x_t^{(j)} \ , \tag{4}$$

so that an observation of a time series at time t will equal the sum of all its components at time t. It is common practice to break such a decomposition down in transitory and persistent components (Beveridge & Nelson, 1981). A transitory component at scale j and time t, denoted as $\hat{x}_t^{(j)}$, represents cyclical movements with a frequency between 2^{j-1} and 2^j years, while a persistent component at scale j and time t, or $\pi_t^{(j)}$, can be viewed as a moving average of the remainder series after all transitory effects up to scale j have been taken into account. Breaking down this decomposition, we have

[2]Online Supplement Bandi et al. (2019)

$$x_t = \underbrace{\frac{x_t - x_{t-1}}{2}}_{\hat{x}_t^{(1)}} + \underbrace{\frac{x_t + x_{t-1}}{2}}_{\pi_t^{(1)}} \tag{5}$$

$$= \underbrace{\frac{x_t - x_{t-1}}{2}}_{\hat{x}_t^{(1)}} + \underbrace{\frac{x_t + x_{t-1} - x_{t-2} - x_{t-3}}{4}}_{\hat{x}_t^{(2)}} + \underbrace{\frac{x_t + x_{t-1} + x_{t-2} + x_{t-3}}{4}}_{\pi_t^{(2)}} , \tag{6}$$

which is equivalent to Section 5 in Bandi et al. (2019). Intuitively, a persistent component at scale $j-1$ can be broken down into a transitory component at scale j and a persistent component at scale j. Bandi et al. (2019) formally denote this property by stating that

$$\hat{x}_t^{(j)} = \pi_t^{(j-1)} - \pi_t^{(j)} , \tag{7}$$

where

$$\pi_t^{(j)} = \frac{\sum_{i=0}^{2^j-1} x_{t-i}}{2^j} . \tag{8}$$

As Ortu et al. (2013) state, computing the transitory and persistent components will lead to overlapping moving averages (read: persistent components), which could lead to biased persistence and serial correlation in the decomposed components. Besides, we note that component-wise observation $\hat{x}_t^{(j)}$ is a linear combination of 'regular' observations x_t to x_{t-2^j+1}. Therefore, to form non-overlapping scale-specific observations, henceforth called *decimated* observations, one should focus on the subseries

$$\left\{\hat{x}_t^{(j)};\ t = k2^j,\ k \in \mathbb{Z}\right\} , \tag{9}$$

$$\left\{\pi_t^{(j)};\ t = k2^j,\ k \in \mathbb{Z}\right\} , \tag{10}$$

so that, with sample size T, the number of scale-specific decimated observations for scale j equals $\lfloor T/2^j \rfloor$. These points can be recovered from (8), however, common practice is the use of an operator matrix which can be used to immediately reconstruct decimated points from regular observations and vice versa. In the case of Bandi et al. (2019), the operator matrix is chosen to be the Haar matrix, so that the transformation of regular to decimated points follows a Discrete Wavelet (Haar) Transform. For the case $J = 2$, this is illustrated by

$$\begin{pmatrix} \pi_t^{(2)} \\ \hat{x}_t^{(2)} \\ \hat{x}_t^{(1)} \\ \hat{x}_{t-2}^{(1)} , \end{pmatrix} = \begin{pmatrix} \frac{1}{2} & \frac{1}{2} & \frac{1}{2} & \frac{1}{2} \\ \frac{1}{2} & \frac{1}{2} & -\frac{1}{2} & -\frac{1}{2} \\ \frac{1}{\sqrt{2}} & -\frac{1}{\sqrt{2}} & 0 & 0 \\ 0 & 0 & \frac{1}{\sqrt{2}} & -\frac{1}{\sqrt{2}} \end{pmatrix} \begin{pmatrix} x_t \\ x_{t-1} \\ x_{t-2} \\ x_{t-3} \end{pmatrix} , \tag{11}$$

or, inversely,

$$\begin{pmatrix} x_t \\ x_{t-1} \\ x_{t-2} \\ x_{t-3} \end{pmatrix} = (T^{(2)})^{-1} \begin{pmatrix} \pi_t^{(2)} \\ \hat{x}_t^{(2)} \\ \hat{x}_t^{(1)} \\ \hat{x}_{t-2}^{(1)} \end{pmatrix}, \tag{12}$$

where $T^{(2)}$, which is the Haar matrix for $J = 2$, is the 4×4 matrix in (11). From the above transform, it can be seen that decimation allows us to completely reconstruct an original time series from only a few points. In this transform, (11) - (12) slightly deviates from the system presented in Section 5 of Bandi et al. (2019), in the sense that we scale the Haar matrix $T^{(2)}$ by a certain factor. This is done to make sure that the Haar matrix is orthonormal, so that the 'unit energy' property (Lindsay, Percival, & Rothrock, 1996) of wavelets is satisfied. As (11) is directly related to (8), the latter equation should be scaled in a similar fashion. This leaves us with

$$\pi_t^{(j)} = \frac{\sum_{i=0}^{2^j-1} x_{t-i}}{\sqrt{2^j}} \ . \tag{13}$$

Note that the above equation, in combination with (7), is not restricted to a certain choice of J. Therefore, the coefficients in the Haar matrix $T^{(J)}$, for arbitrary J, can simply be derived from the coefficients of linear combinations in (7) and (13), following a similar procedure as that of Ortu et al. (2013). The case $J = 4$, which is employed for the empirical data, is elaborated on in Appendix D. Furthermore, the Haar matrix $T^{(J)}$ is orthogonal, so that components should be uncorrelated across scales. The obtained decimated observations (9), for $j = 1, ..., J$ and series r_t and v_t, can be used to both model and evaluate scale-specific predictability. A data generating process, following Bandi et al. (2019), based on frequency-wise modelling can be depicted (for scale j) by

$$r_{k2^j+2^j}^{(j)} = \beta_j v_{k2^j}^{(j)} + u_{k2^j+2^j}^{(j)} \ , \tag{14}$$

$$v_{k2^j+2^j}^{(j)} = \rho_j v_{k2^j}^{(j)} + e_{k2^j+2^j}^{(j)} \ , \tag{15}$$

where r and v denote returns and variance respectively, while u and e are white noise shocks. The above system will be referred to when simulating a scale-specific system. When the interest is merely evaluating scale-specific predictability, performing the regression (14) suffices.

Due to the structure of the Haar transform, there exists a one-to-one relation between regular and decimated observations; the one can directly be transformed into the other. Therefore, when modelling decimated observations and translating these into regular observations, one can once again perform aggregated regressions to evaluate the behavior of regression slopes and coefficients

of determination. When the scale-specific DGP (14) - (15) is constructed so that predictability ($\beta_j \neq 0$) occurs at scale j^* only, Proposition I (Bandi et al., 2019) state that a predictive peak in two-way aggregated regressions should occur at horizon $h = 2^{j^*}$. Thus, setting $j^* = 4$, a peak in predictability should occur at a horizon of 16 years, which, in the case of corresponding hump-shaped behavior, would be in consistence with the empirical results of Bandi et al. (2019). To verify whether the data generating process (14) - (15) can in fact recover hump-shaped behavior from decimated observations, we use simulation. Specifics for this simulation can be found in Appendix H or part B of the Online Supplement of Bandi et al. (2019).

4.2 Extension

Besides reviewing Bandi et al. (2019), this paper provides three extensions.

4.2.1 Robustness Analysis

It might be probable that slight changes in the data have a large effect on the conclusions drawn based on scale-specific predictability relations. To investigate this sensitivity, this research will make slight adjustments to establish robustness. Firstly, a change in data is employed by using the S&P 500 instead of the NYSE/AMEX index for market returns and realized variance. In this case, the methods for aggregation and scale-specific predictability discussed in Section 4.1 remain exactly the same. Secondly, the sample period is, as described in Section 2, adjusted to the post-war period, as structural change during the Great Depression or World War II may have taken place. The sample used in this analysis will commence in 1951. Thirdly, the behavior of aggregated regressions when varying the horizon over which frequencies are measured between regressand and regressor is investigated. I do so by considering all possible combinations of horizons ($H = 20$) and evaluating their R^2's. A similar approach can be taken for scale-specific predictability, in which the assumption of equal scale j for both $r_t^{(j)}$ and $v_t^{(j)}$ in (14) was made. Leaving out this assumption, we may perform predictive regressions for all possible combinations of scales for returns and variance (with $J = 4$).

4.2.2 High-frequency Analysis

It may be possible that altering the aggregation horizon, as in Section 4.2.1, leads to the conclusion that predictability peaks occur at a horizon larger than 16 years. However, the framework of Bandi et al. (2019) merely allows us to model returns and variance for frequencies up to 16 years, as increasing the scale, e.g. $J = 5$, would imply that the number of decimated observations for this

scale reduces to $\lfloor T/32 \rfloor = 2$ observations (as the maximum sample size $T = 93$). In this case, predictive regressions on decimated components would thus not be informative. To solve this issue, changing the frequency of data sampling might prove to be a solution.

This section therefore investigates monthly instead of yearly observations. For scale j, movements with cycles between 2^{j-1} and 2^j months are thus included. This analysis constitutes the NYSE/AMEX, S&P 500, AEX and FTSE 100 index. Due to interest rate availability and the establishment of the latter two indices in 1983 and 1984 respectively, the sample period for the first two indices ranges from 1933 to 2018 ($T = 1024$), while the sample size of the AEX and FTSE 100 equals 532 and 526 respectively. Because of the difference in sample size, $J = 8$ for the NYSE/AMEX and S&P 500, while $J = 6$ for the AEX and FTSE 100. An overview of the frequencies belonging to each scale is provided in Table 7 of Appendix C.

4.2.3 Multiple Regressor System

Besides altering frequencies, the scale-specific system can be expanded into higher dimensions by adding multiple regressors next to the variance. As described in Section 3, these regressors include the dividend yield and inflation.

The forward/backward aggregated regression (1) can be generalized by writing

$$\sum_{i=t+1}^{t+h} r_{t+1,t+h} = \alpha_h + \beta_{1,h} \sum_{i=t+1}^{t+h} x_{1,i-h} + \beta_{2,h} \sum_{i=t+1}^{t+h} x_{2,i-h} + ... + \beta_{M,h} \sum_{i=t+1}^{t+h} x_{M,i-h} + \sum_{i=t+1}^{t+h} \epsilon_i \ , \quad (16)$$

with $x_{m,t}$ regressor $m = 1, ..., M$, while t runs, just as in (1), from h to $T - h$. As with (1), we can perform the above regression and evaluate its coefficients and R^2.

In similar fashion, we may extend this multivariate framework into scale-specific relations, so that the predictive relationship (14) can be written as

$$r^{(j)}_{k2^j+2^j} = \beta_{1,j} x^{(j)}_{1,k2^j} + \beta_{2,j} x^{(j)}_{2,k2^j} + ... + \beta_{M,j} x^{(j)}_{M,k2^j} + u^{(j)}_{k2^j+2^j} \ , \quad (17)$$

where $x^{(j)}_{m,k2^j}$ is a decimated point at scale j and time $k2^j$ (with $k \in \mathbb{Z}$) for predictor $m = 1, ..., M$. For each scale, regression (17) can directly be employed to investigate scale-specific predictability. The decimated returns and predictors can once again be retrieved from using either a Haar transform or relation (13), for the latter of which one should make sure observations are non-overlapping, see support (9) - (10).

5 Results

In the following, the results of this research will be presented in the same order as Section 4. Note that these results differ from those presented by Bandi et al. (2019); this is due to slight discrepancies in data and methods used. For a detailed explanation and discussion, the reader is referred to Appendices A and I.

5.1 Replication

As with Section 4.1, this section can be divided into an analysis of aggregated regressions and scale-specific modelling.

5.1.1 Aggregated Regressions

Performing the two-way aggregated regressions (1) based on returns from the NYSE/AMEX index and the three variance proxies described in Section 3, the coefficients of determination for a horizon up to $H = 20$ years are illustrated in Figure 1. As in Bandi et al. (2019), the R^2 of the three variance proxies all exhibit an upwards trend in the first years, leading up to a peak, after which a decrease kicks in; the so-called 'hump-shaped' behavior. As opposed to the findings in Bandi et al. (2019), Figure 1 shows that the R^2 for the market variance is highest when $h = 17$. Therefore, the empirical peak would not occur at scale $j = 4$, which contains movements between 8 and 16 years (Table 7) but rather at scale $j = 5$. For the consumption variance and EPU proxy, peaks occur at $h = 13$ and $h = 16$ years respectively. The peaks for these graphs lie around 60%, therewith slightly higher than the 55% as presented by Bandi et al. (2019).

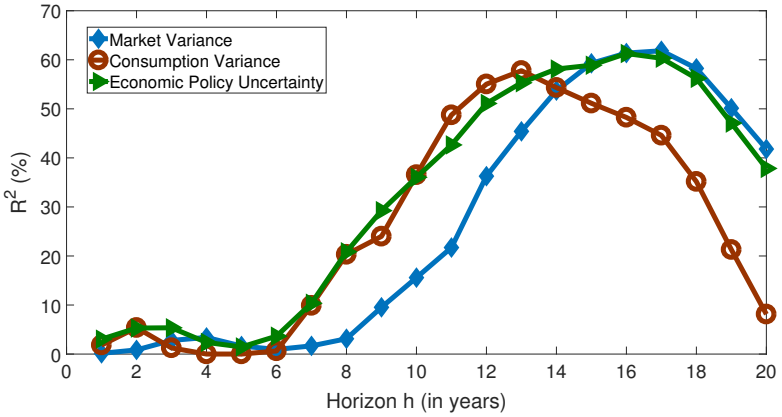

Figure 1: Plot of the R^2's for two-way aggregated regressions of excess market returns on market variance, consumption variance and economic policy uncertainty for the NYSE/AMEX index.

Besides the R^2, Table 1 provides slopes and corresponding t-statistics (Newey-West and Valkanov, 2003) based on the forward/backward aggregated regressions of excess market returns on market variance. From this table, it becomes clear that the regression slope exhibits some sort of hump-shaped behavior as well, with a peak occurring at $h = 15$. In Bandi et al. (2019), $h = 16$ leads to the highest slope, while the magnitude of their slopes is larger than that in Table 1. Similar tables can be constructed for the Consumption Variance and EPU proxies, for which similar hump-shaped behavior in slopes and R^2's holds. Therefore, we do not discuss these tables separately, but both are provided in Appendix E.

Table 1: Table containing properties for forward/backward regressions (1) of NYSE/AMEX returns on market variance over horizon h. Panels A1 and A2 contain slope estimates (b), Newey-West t-statistics (NW), Valkanov (2003) t-statistics and R^2's

Panel A1: $r_{t+1,t+h} = \alpha_h + \beta_h v_{t-h+1,t} + \epsilon_{t+1,t+h}$										
h	1	2	3	4	5	6	7	8	9	10
b	0.192	0.366	0.558	0.467	0.285	0.200	0.253	0.346	0.619	0.823
NW	0.281	0.630	1.722	1.542	0.854	0.587	0.760	1.019	1.795	2.364
Valkanov	0.038	0.091	0.167	0.185	0.128	0.096	0.129	0.177	0.320	0.424
R^2 (%)	0.148	0.846	2.784	3.389	1.642	0.942	1.671	3.126	9.534	15.584
Panel A2: $r_{t+1,t+h} = \alpha_h + \beta_h v_{t-h+1,t} + \epsilon_{t+1,t+h}$										
h	11	12	13	14	15	16	17	18	19	20
b	0.998	1.311	1.488	1.647	1.748	1.729	1.675	1.547	1.376	1.172
NW	3.017	4.131	4.914	6.189	8.055	9.021	9.925	9.385	8.131	6.236
Valkanov	0.519	0.744	0.899	1.061	1.188	1.240	1.252	1.161	0.984	0.832
R^2 (%)	21.717	36.272	45.409	53.716	59.285	61.373	61.838	58.251	50.126	41.801

As described in Section 4.1, classical predictive systems (2) - (3) should not be able to replicate the hump-shaped behavior as observed in Figure 1. This is confirmed using Simulation A, see Appendix F. From simulating classical predictive systems and correspondingly forward/backward aggregating returns and variance, it follows that both R^2 and β are hump-shaped in only 2.17% of the simulated regressions. This number even decreases to under 1% when also imposing the restriction that the maximum of R^2 should exceed 50%, as it does in the empirical case. It is thus hard to argue that classical predictive systems are able to have long-run predictability following a tent-shaped pattern.

5.1.2 Scale-specific Framework

Now turning to the scale-specific framework, we may begin with investigating the four separate components. For these four components based on excess market returns, the decimated points, constructed by means of the normalized discrete Haar transform (Appendix D), and 'redundant' calendar-time scale-specific points, constructed by means of (13), are plotted in Figure 2. The calendar-time specific points are redundant, as all information about the regular time series is already

captured in the few decimated points. Similar decompositions can be made for the three variance proxies, which are not given in this paper.

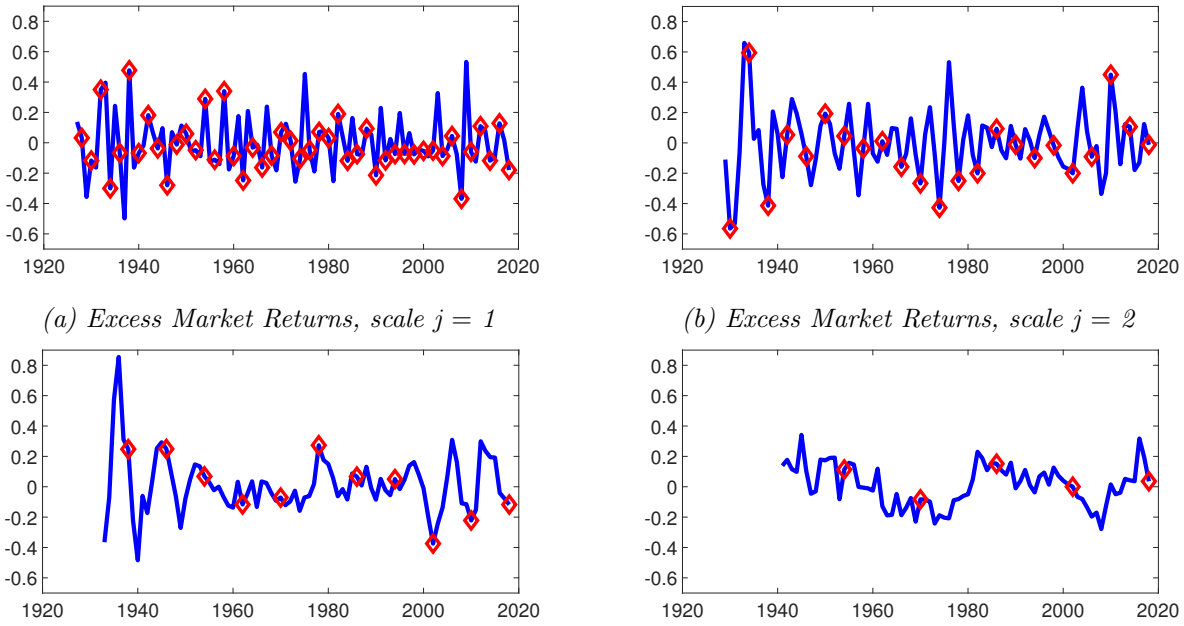

(a) Excess Market Returns, scale $j = 1$

(b) Excess Market Returns, scale $j = 2$

(c) Excess Market Returns, scale $j = 3$

(d) Excess Market Returns, scale $j = 4$

Figure 2: Graphs of the decomposed series of excess market returns for the NYSE/AMEX market index over time. The solid (blue) lines represent scale-specific calendar-time observations, while the (red) diamonds constitute decimated observations.

As a consequence of the wavelet decomposition of the scale-specific framework from Section 4.1, decimated observations from different scales should be uncorrelated. To investigate whether this property goes up empirically, we compute correlations across scales. Note that these correlations are calculated based on the redundant, overlapping data, so that the same, reasonably large, number of observations can be established for each scale. As calculation of a scale-specific calendar-time point at time t via (13) requires knowledge of the regular time series from time t to time $t - 2^j + 1$, we compute correlations by leaving out the first $2^J - 1$ periods. The corresponding correlations are provided in Table 2.

Table 2: Pairwise correlations between separate components based on redundant, overlapping observations for excess market returns, market variance, consumption variance and economic policy uncertainty (EPU). The returns and market variance come from the NYSE/AMEX index.

	Returns			**Market Variance**			**Consumption Variance**			**EPU**		
Scale j	2	3	4	2	3	4	2	3	4	2	3	4
1	-0.03	-0.01	0.12	0.15	-0.08	0.02	0.01	0.06	-0.07	0.19	-0.04	-0.01
2		-0.09	0.15		0.09	0.07		0.09	-0.20		0.21	0.06
3			0.12			0.25			-0.07			0.39

From Table 2, it follows that most pairwise correlations are low, which is in consistence with theory. Some correlations are relatively high, which may be a consequence of leakage occurring between scales due to the overlapping of observations (however, one should evaluate significance of these correlations to make defnitive inferences). Having looked at the (decimated) components, we may now investigate predictability. Performing predictive regressions (14) for each scale separately, taking decimated points as inputs, leads to Table 3. As the regressions are predictive, a regression for scale j contains $\lfloor T/2^j \rfloor - 1$ observations. From Table 3, one can see that the R^2 is highest for $j = 4$ for all three variance proxies, which is in correspondence with Bandi et al. (2019). The corresponding values furthermore resemble those depicted in Figure 1 quite neatly, taking into account that the three respective graphs have an R^2 that reaches around 60% at its peak.

Table 3: Predictive regressions of the components of excess market returns on each of the variance proxies separately. The table reports coefficient estimates, t-statistics and R^2's for each regression using the NYSE/AMEX index in Panel A and the S&P 500 index in Panel B.

$$\mathrm{r}^{(j)}_{k2^j+2^j} = \beta_j v^{(j)}_{k2^j} + u^{(j)}_{k2^j+2^j}$$

Panel A: NYSE/AMEX					**Panel B:** S&P 500				
Market Variance									
Scale j	1	2	3	4	*Scale j*	1	2	3	4
$\hat{\beta}_j$	-1.07	3.10	-0.88	3.20	$\hat{\beta}_j$	-1.13	2.58	-0.72	2.10
t-stat	-1.13	1.86	-0.86	1.00	t-stat	-1.32	2.01	-0.87	0.89
R^2 (%)	4.49	16.14	8.48	42.95	R^2	5.33	17.78	11.01	40.49
Consumption Variance									
Scale j	1	2	3	4	*Scale j*	1	2	3	4
$\hat{\beta}_j$	-6.05	-9.71	-3.47	2.09	$\hat{\beta}_j$	-7.18	-9.67	-3.31	2.46
t-stat	-1.29	-2.67	-0.96	3.51	t-stat	-1.47	-2.74	-0.86	5.34
R^2 (%)	7.60	29.69	11.49	73.35	R^2	8.28	30.69	11.30	86.42
EPU									
Scale j	1	2	3	4	*Scale j*	1	2	3	4
$\hat{\beta}_j$	-0.04	-0.09	-0.06	0.06	$\hat{\beta}_j$	-0.04	-0.09	-0.06	0.06
t-stat	-1.16	-1.25	-2.13	1.55	t-stat	-1.26	-1.35	-2.03	1.63
R^2 (%)	5.37	6.73	33.86	56.39	R^2	5.67	7.74	33.26	59.53

To investigate whether the results in Table 3, or the scale-wise framework in general, are in consistence with the behavior of R^2 in forward/backward aggregated regressions, simulations are again taken out. These show that some type of double-hump arises; the R^2 increases until reaching a peak around $h = 7$ years, after which a decrease kicks in. From $h = 10$ onwards, R^2 rises again before reaching an ultimate peak at $h = 16$. Although results are provided in Appendix H, it becomes clear that the hump-shaped behavior fits not all too badly with the scale-specific system. The percentage of simulations for which both R^2 and β are hump-shaped lies around 17.6%. When imposing the restriction that the R^2 should reach over 50%, still 13.28% satisfies this restriction.

5.2 Extension

This section will start off with a robustness analysis, after which higher-frequency data and systems with multiple regressors are analyzed.

5.2.1 Robustness Analysis

The first adjustmentis that of using a returns from the S&P 500 instead of the NYSE/AMEX market index. By performing forward/backward aggregated regressions for all three variance proxies, Figure 3a is obtained. As this figure shows, using S&P 500 does not change the hump-shaped behavior in any meaningful way, so that predictive peaks with an R^2 approaching 60% occur around a horizon of 16 years. In this case, the predictive peak for the market variance proxy is situated at $h = 16$, instead of $h = 17$, as was the case in Figure 1.

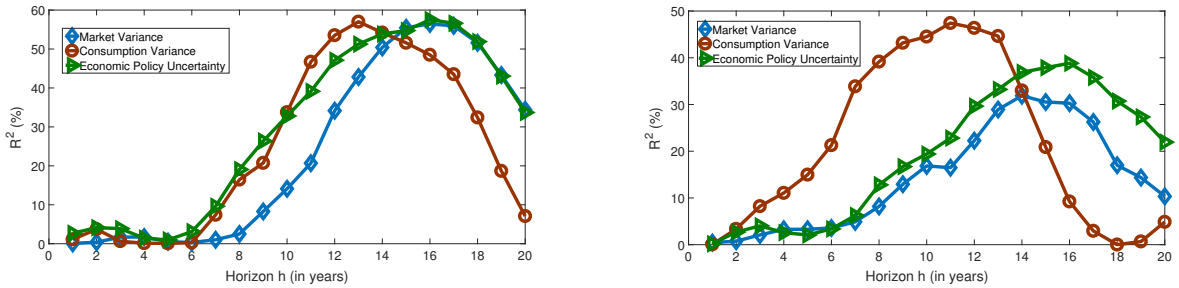

(a) S&P 500. *(b) Post-war period, NYSE/AMEX.*

Figure 3: Plot of the R^2's for two-way aggregated regressions of excess market returns on market variance, consumption variance and economic policy uncertainty for the S&P 500 index (left) and the post-war period using the NYSE/AMEX index (right).

Panel B of Table 3 contains properties of scale-specific predictive regressions for the S&P 500 index. As with the NYSE/AMEX index, the R^2 is highest for regressions for component $j = 4$. Besides, the differences in R^2 and slope estimates are only slight between the two indices. Therefore, one could say that changing the market index to the S&P 500 does not change the findings in any meaningful way, so that the results are relatively robust to the choice of index. Therefore, we will stick with the NYSE/AMEX index in the remainder of this section.

To further investigate sensitivity, consider the post-war sample period commencing in 1951. For this sample period, a graphical representation of the R^2 of forward/backward aggregated regressions is to be found in Figure 3. Again, the graphs of all three variance proxies seem to be in line with the hump-shaped behavior, although the predictability peaks are relatively low. The coefficients of determination for scale-specific regressions (14) show a similar pattern (see Table 4), with peaks for

$j = 4$, although the R^2's at these peaks are not as high as in the case of the larger sample. As the sample size is reduced, the reliability of the predictive regressions deteriorates, so that one should not focus too much on the results presented in Table 4.

Table 4: Table containing the R^2 (%) of scale-specific predictive regressions for the post-war sample, based on returns from the NYSE/AMEX index

R^2 of regression: $r^{(j)}_{k2^j+2^j} = \beta_j v^{(j)}_{k2^j} + u^{(j)}_{k2^j+2^j}$				
Scale j	1	2	3	4
Market Variance	4.98	12.98	6.63	19.11
Consumption Variance	8.94	15.69	21.13	24.87
Economic Policy Uncertainty	5.15	17.29	22.11	47.56

The third and final part of this sensitivity analysis consists of analyzing the interactions between return- and variance-specific aggregation horizons. By considering all possible combinations of horizons (while keeping $H = 20$) for regressand and regressor, we may find the 'best' predictive relation. These relations are provided in Table 5. From this table, we can deduct that the 'optimal' combination of aggregation horizons for returns and variance i) does not necessarily occur at the same horizon, and ii) does not necessarily lie within the perks of $J = 4$. As monthly (high-frequency) analysis allows us to separate frequencies reaching over 20 years, this analysis seems highly relevant.

Table 5: Table that gives the unrestricted (optimal lags) and restricted (equal lags) best combinations of aggregation horizons for variance and returns, as measured by R^2 in forward/backward regressions for NYSE/AMEX returns and the three variance proxies.

	Market Variance		**Consumption Variance**		**EPU**	
	Optimal lags	*Equal lags*	*Optimal lags*	*Equal lags*	*Optimal lags*	*Equal lags*
$[h_{variance}, h_{returns}]$	[14, 20]	[17, 17]	[12, 14]	[13, 13]	[11, 20]	[16, 16]
R^2 (%)	65.23	61.84	60.76	57.78	75.63	61.28

Before turning to the high-frequency analysis, we may note that component-wise predictive regressions could yield a 'best' predictive model when regressand and regressor do not follow the same scale. However, it turns out that choosing $j = 4$ for both returns and variance (all three proxies) yields the highest R^2 from all possible combinations.

5.2.2 High-frequency Analysis

As explained in section 4.2.2, we investigate the behavior of (scale-specific) predictability using monthly returns instead of yearly returns as a basis. In doing so, I make use of the NYSE/AMEX, S&P 500, FTSE 100 and AEX indices. The results of two-way aggregated regressions for these indices of excess market returns on market variance over horizon h is provided in Figure 4a. In this graph, we let h run from 1 to 250 months (just over 20 years). Note that the graphs for the FTSE

100 and AEX 'stop' at $h = 200$. This is due to only having a limited amount of data points for these two indices. In consistence with the yearly patterns, hump-shaped behavior is present with a peak around 16 years ($h = 192$) for the S&P 500 and a peak around 17 years ($h = 204$) for the NYSE/AMEX index. Especially the latter is interesting, as a frequency of 17 years was not included in the yearly fourth scale. For the FTSE 100 and AEX, there seems to be some kind of hump when looking at the first 160 months. However, from $h = 160$ to $h = 180$, the R^2 of aggregated regressions for both indices increases sharply, leading to some kind of double-hump with peaks reaching over 80%. One could note that the regressions for h large, e.g. 180, are not too reliable due to the small amount of data. However, Figure 4a still shows that hump-shaped behavior for the FTSE 100 and AEX may not be present.

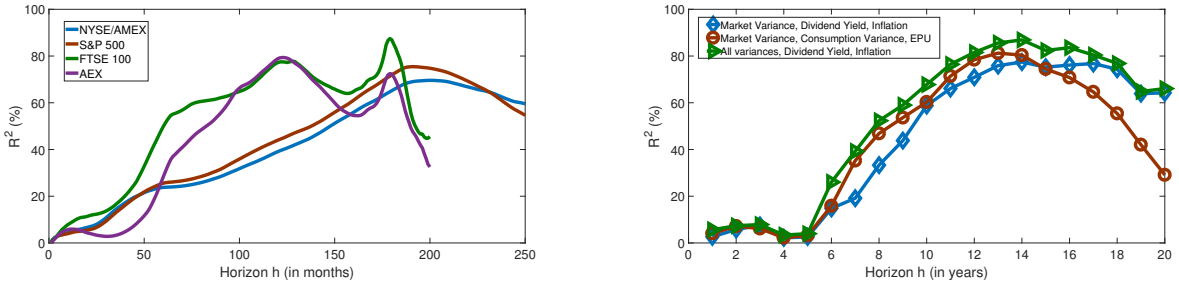

(a) Monthly frequency. *(b) Multiple regressors.*

Figure 4: Plot of the R^2's for two-way aggregated regressions over horizon h of excess market returns on market variance for the NYSE/AMEX, S&P 500, FTSE 100 and AEX (left). Plot of the R^2's for two-way aggregated regressions of excess market returns on i) market variance, inflation rate and dividend yield, ii) consumption variance, inflation rate and dividend yield, iii) EPU, inflation rate and dividend yield, and iv) market variance, consumption variance, EPU, inflation rate and dividend yield (right).

To investigate scale-specific behavior, we perform predictive regressions (14), where we take $J = 8$ for the NYSE/AMEX and S%P 500. Fo the FTSE 100 and AEX, $J = 6$ would be the maximum number of scales (to ensure the number of decimated points for each scale remains sufficiently large), so that we could merely look at frequencies up to 64 months or $5\frac{1}{3}$ years, which would not be too informative. For the predictive regressions, we thus focus on the NYSE/AMEX and S&P 500 index. Table **??** reports coefficient estimates, along with t-statistics and R^2's for each scale separately. The R^2's correspond well with the patterns observed in Figure 4a, in the sense that the peak occurs at the highest scale with an R^2 of around 70%. To investigate whether the above patterns follow from actual predictability or mere spurious behavior, one could again perform simulations. However, due to the significance of coefficient estimates and more specific filtering, this would not be expected. Performing such simulations is left for future research.

Table 6: Coefficient estimates, their t-statistics, and the R^2 of scale-wise predictive regressions of excess returns on market variance for scales $j = 1$ to $j = 8$, using the NYSE/AMEX or S&P 500.

NYSE: $r^{(j)}_{k2^j+2^j} = \beta_j v^{(j)}_{k2^j} + u^{(j)}_{k2^j+2^j}$								
Scale j	1	2	3	4	5	6	7	8
$\hat{\beta}_j$	1.04	1.00	0.37	-0.94	-2.08	0.00	-0.47	18.19
t-stat	1.38	0.98	0.49	-0.57	-1.48	0.00	-0.13	1.73
R^2 (%)	0.38	2.50	0.27	2.51	7.93	8.77	12.04	68.28
SP: $r^{(j)}_{k2^j+2^j} = \beta_j v^{(j)}_{k2^j} + u^{(j)}_{k2^j+2^j}$								
Scale j	1	2	3	4	5	6	7	8
$\hat{\beta}_j$	0.71	0.88	0.62	-0.85	-1.85	0.16	-0.61	13.67
t-stat	1.04	1.02	0.86	-0.61	-1.47	0.05	-0.20	1.58
R^2 (%)	0.23	2.27	0.58	2.38	7.53	9.41	15.08	65.64

5.2.3 Multiple Regressor System

The final extension, as described in Section 4.2.3, is that of using a multiple regressor system, for which dividend yield and inflation are used as additional predictors besides the variance. Figure 4 plots the R^2 of two-way aggregated regressions for three combinations of predictors included. All three graphs seem to be in line with the hump-shaped behavior reported before, while the predictive peak reaches almost 90%.

We may investigate whether scale-specific predictive regressions are in line with the hump-shaped pattern observed. To do so, we use the redundant scale-specific observations formed by (13) for the system containing all three variance proxies, dividend yield and inflation. We choose this system as its R^2, visible in Figure 4, generally is the highest of the three graphs. We use redundant data to prevent identification issues. As the scale $j = 4$ contains $\lfloor T/2^j \rfloor = 5$ decimated observations, using 5 predictors would lead to over-identification. The scale-specific regressions result in R^2's of 8.80, 9.05, 27.51 and 42.35 % for scale 1 to 4. Extensive results from these predictive regressions are given in Table 16, Appendix G. Although the R^2 is highest for $j = 4$, its magnitude is substantially smaller than that in Figure 4.

6 Conclusion & Discussion

In this paper, the behavior of slopes and coefficients of determination in predictive regressions for returns as presented by Bandi et al. (2019) is first reviewed, after which extensions are applied. In reviewing, the hump-shaped behavior of R^2's in forward/backward aggregated regressions of excess market returns on variance is replicated. By performing simulations, this paper shows that classical predictive systems are unable of capturing the same kind of movements in coefficients of determination of aggregated regressions. Therefore, this research applies scale-specific systems, given by Bandi et al. (2019), to model decomposed time series based on frequencies of cyclical

movements. By means of such decompositions, scale-specific predictability between returns and variance is investigated, for which, in correspondence with Bandi et al. (2019), peaks are found for components with frequencies between 8 and 16 years. Through simulations, this scale-specific behavior fits in well with the observed hump-shaped behavior of aggregated regressions.

By performing robustness analyses, this research analyses the variability of the results of Bandi et al. (2019). Choosing a different data set (S&P 500 instead of NYSE/AMEX index) is shown not to change results in any meaningful way. Adjusting the sample period to the post-war period does not alter the notion of hump-shaped behavior, although the magnitude and location of predictive peaks slightly change. As for the location of peaks, this paper shows that these do not always occur between 8 and 16 year and aggregation horizons do not have to be equal for both returns and variance to maximize R^2. High-frequency analysis allows a separation into a larger amount of scales, while more data points are used. This leads to support of hump-shaped behavior and scale-specific predictability for the NYSE/AMEX and S&P 500 index, while the behavior of the FTSE 100 and AEX is not conclusive and requires further analysis and more data points. By introducing a multiple regressor system, this research provides its final extension. Incorporating dividend yields and inflation rates is shown to not clearly affect hump-shaped behavior, while increasing predictability up to near 90%.

A major drawback of this research and the framework of Bandi et al. (2019) is the number of observations. The maximum sample period includes 93 yearly observations, a number which decreases quickly with the increase of scales. Therefore, one should either find larger data sets, e.g. Lundblad (2007), or find a way to overcome the issue of having few data points. Furthermore, this research could be improved by putting more focus on evaluating significance of estimates, for instance by considering confidence intervals for the R^2 or standard errors for correlations across scales. Lastly, investigating stock markets outside the US with relatively many data points could be investigated, to establish whether hump-shaped behavior is merely a US 'coincidence' or really a 'stylized fact'.

7 Acknowledgements

I would like to thank dr. M. Grith, my supervisor during the process of writing this thesis. Throughout this project, she helped me understand complex abstract concepts and gave valuable feedback. Furthermore, I would like to thank F.M. Bandi, B. Perron, A. Tamoni and C. Tebaldi for their helpful comments and insights, as well as any provided data and code.

References

Andersen, T. G., Bollerslev, T., Diebold, F. X., & Labys, P. (2001). The distribution of realized exchange rate volatility. *Journal of the American statistical association*, *96*(453), 42–55.

Ang, A., & Bekaert, G. (2006). Stock return predictability: Is it there? *The Review of Financial Studies*, *20*(3), 651–707.

Asprem, M. (1989). Stock prices, asset portfolios and macroeconomic variables in ten european countries. *Journal of Banking & Finance*, *13*(4-5), 589–612.

Baker, S. R., Bloom, N., & Davis, S. J. (2016). Measuring economic policy uncertainty. *The quarterly journal of economics*, *131*(4), 1593–1636.

Bandi, F. M., & Perron, B. (2008). Long-run risk-return trade-offs. *Journal of Econometrics*, *143*(2), 349–374.

Bandi, F. M., Perron, B., Tamoni, A., & Tebaldi, C. (2019). The scale of predictability. *Journal of Econometrics*, *208*(1), 120–140.

Bansal, R., Kiku, D., & Yaron, A. (2009). *An empirical evaluation of the long-run risks model for asset prices* (Tech. Rep.). National Bureau of Economic Research.

Baxter, M., & King, R. G. (1999). Measuring business cycles: approximate band-pass filters for economic time series. *Review of economics and statistics*, *81*(4), 575–593.

Beveridge, S., & Nelson, C. R. (1981). A new approach to decomposition of economic time series into permanent and transitory components with particular attention to measurement of the 'business cycle'. *Journal of Monetary economics*, *7*(2), 151–174.

Bollerslev, T., Osterrieder, D., Sizova, N., & Tauchen, G. (2013). Risk and return: Long-run relations, fractional cointegration, and return predictability. *Journal of Financial Economics*, *108*(2), 409–424.

Campbell, J. Y. (1991). A variance decomposition for stock returns. *The economic journal*, *101*(405), 157–179.

Chen, S.-S. (2009). Predicting the bear stock market: Macroeconomic variables as leading indicators. *Journal of Banking & Finance*, *33*(2), 211–223.

Cochrane, J. H. (2007). The dog that did not bark: A defense of return predictability. *The Review of Financial Studies*, *21*(4), 1533–1575.

Cochrane, J. H. (2009). *Asset pricing: Revised edition*. Princeton university press.

Comin, D., & Gertler, M. (2006). Medium-term business cycles. *American Economic Review*, *96*(3),

523–551.

Daniel, K., & Torous, W. (1991). Common stock returns and the business cycle.

Ding, Z., Granger, C. W., & Engle, R. F. (1993). A long memory property of stock market returns and a new model. *Journal of empirical finance*, *1*(1), 83–106.

Fama, E. F., & French, K. R. (1988). Dividend yields and expected stock returns. *Journal of financial economics*, *22*(1), 3–25.

Fama, E. F., & French, K. R. (1989). Business conditions and expected returns on stocks and bonds. *Journal of financial economics*, *25*(1), 23–49.

Fama, E. F., & Schwert, G. W. (1977). Asset returns and inflation. *Journal of financial economics*, *5*(2), 115–146.

French, K. R., Schwert, G. W., & Stambaugh, R. F. (1987). Expected stock returns and volatility. *Journal of financial Economics*, *19*(1), 3–29.

Ghysels, E., Santa-Clara, P., & Valkanov, R. (2005). There is a risk-return trade-off after all. *Journal of Financial Economics*, *76*(3), 509–548.

Ghysels, E., Santa-Clara, P., & Valkanov, R. (2006). Predicting volatility: getting the most out of return data sampled at different frequencies. *Journal of Econometrics*, *131*(1-2), 59–95.

Goyal, A., & Santa-Clara, P. (2003). Idiosyncratic risk matters! *The Journal of Finance*, *58*(3), 975–1007.

Lee, G. G., & Engle, R. F. (1993). A permanent and transitory component model of stock return volatility. *Available at SSRN 5848*.

Lewellen, J. (2004). Predicting returns with financial ratios. *Journal of Financial Economics*, *74*(2), 209–235.

Lindsay, R. W., Percival, D. B., & Rothrock, D. (1996). The discrete wavelet transform and the scale analysis of the surface properties of sea ice. *IEEE Transactions on Geoscience and Remote Sensing*, *34*(3), 771–787.

Lundblad, C. (2007). The risk return tradeoff in the long run: 1836–2003. *Journal of Financial Economics*, *85*(1), 123–150.

Müller, U. K., & Watson, M. W. (2008). Testing models of low-frequency variability. *Econometrica*, *76*(5), 979–1016.

Nelson, D. B. (1991). Conditional heteroskedasticity in asset returns: A new approach. *Econometrica: Journal of the Econometric Society*, 347–370.

Ortu, F., Severino, F., Tamoni, A., & Tebaldi, C. (2017). A persistence-based wold-type decompo-

sition for stationary time series. *Available at SSRN 1973049*.

Ortu, F., Tamoni, A., & Tebaldi, C. (2013). Long-run risk and the persistence of consumption shocks. *The Review of Financial Studies*, *26*(11), 2876–2915.

Patelis, A. D. (1997). Stock return predictability and the role of monetary policy. *the Journal of Finance*, *52*(5), 1951–1972.

Tamoni, A. (2011). The multi-horizon dynamics of risk and returns.

Torous, W., & Valkanov, R. (2000). Boundaries of predictability: Noisy predictive regressions.

Valkanov, R. (2003). Long-horizon regressions: theoretical results and applications. *Journal of Financial Economics*, *68*(2), 201–232.

Welch, I., & Goyal, A. (2007). A comprehensive look at the empirical performance of equity premium prediction. *The Review of Financial Studies*, *21*(4), 1455–1508.

Yogo, M. (2008). Measuring business cycles: A wavelet analysis of economic time series. *Economics Letters*, *100*(2), 208–212.

Zarnowitz, V., & Ozyildirim, A. (2006). Time series decomposition and measurement of business cycles, trends and growth cycles. *Journal of Monetary Economics*, *53*(7), 1717–1739.

A Excess Market Returns Data

Before delving into a detailed description on the used data for excess market returns, I would like to note that I received code and data from the authors. Consequently, I will both explain my own thoughts and the implementation of the authors. As you will note, there are some discrepancies between the methods Bandi et al. (2019) use and the ones I pursue. The sample period used by Bandi et al. (2019) ranges from 1930 to 2014.

As noted in Appendix B of Bandi et al. (2019), the excess market returns are defined as the difference between the continuously compounded market returns and risk-free rate. Section 3 notes that the market returns are obtained as the NYSE/AMEX monthly value-weighted index including dividends from the Chicago Center for Research in Security Prices (CRSP). Although the data I obtained from the CRSP are exactly similar to the data of Bandi et al. (2019) for the period 1930 - 1972, differences arise afterwards. This discrepancy is most likely explained by the fact that Bandi et al. (2019) obtained their data some time ago, such that the data series might have been adjusted slightly.

Most logically, one would transform these monthly data to annual continuously compounded data by using

$$r_y = \sum_{m=1}^{12} ln(1 + r_{m,y}) \qquad y = 1, ..., Y \ , \tag{18}$$

where y and m respectively denote year and month, while r is a simple return. The above equation states that annual continuously compounded returns equal the sum of monthly continuously compounded returns in a year. This is the approach that I will take in annualising data, but the approach of Bandi et al. (2019) deviates from this method a bit.

The method Bandi et al. (2019) use, rests on restructuring the data so that dividend yield and capital gains yield are separated. To do so, Bandi et al. (2019) obtain monthly returns excluding dividends via the CRSP. By combining the returns including and the returns excluding dividends, the price index and dividend are calculated for each time, after which Bandi et al. (2019) form monthly simple returns by means of

$$r_{m,y} = \frac{D_{m,y} + P_{m,y}}{P_{m,y-1}} \qquad m = 1, ..., 12 \ , \ y = 1, ..., Y \ , \tag{19}$$

where $D_{m,y}$ and $P_{m,y}$ are the dividends and price index in month m of year y respectively. Intuitively, the above approach should in the end deliver simple returns that are exactly equal to the value-

weighted return including dividends, but, as the data file sent by the authors suggests, this is not the case. In Appendix J I include a derivation which proves that both returns should be equal. Therefore, the discrepancies between the returns are most likely due to rounding errors. In this paper, I stick to using the value-weighted returns including dividends as readily obtained from the CRSP and thus do not persuade the transformation of Bandi et al. (2019).

The annualized returns via (18) are nominal returns, i.e. inflation is not taken account for. However, to compare returns over the years, we should be using real returns. These real returns can be computed by

$$r_{real,t} = r_{nom,t} - r_{infl,t} \ , \tag{20}$$

so that real returns equal nominal returns minus inflation at time t. The inflation data are obtained once again via CRSP as the annual rate of change of the Consumer Price Index. Bandi et al. (2019) obtain their inflation data via monthly CPI numbers from the Bureau of Labor Statistics (BLS) and consequently calculate the change of the December CPI of consecutive years. This results in exactly the same numbers as those from the CRSP. As we are working with continuously compounded returns, I transform the simple inflation data by means of

$$r_{infl,t} = ln(1 + R_{infl,t}) \ , \tag{21}$$

where r is the continuously compounded inflation, while R is the simple inflation.

Now subtracting inflation from annual market returns, we obtain real annual market returns. However, we are interested in the excess returns. Therefore, we need to involve the risk-free rate in these computations. Data on the risk-free rate is obtained from the Federal Reserve Economic Data (FRED) and contains monthly data from 1934 to 2014. The annual risk-free rate is taken to be the risk-free rate in December of the respective year. This is not equal to the end-of-year rate, as FRED T-bill data is reported on the first day of a month. Therefore, the risk-free rate in a year equals the risk-free rate on the 1st of December of the respective year. For the period 1930 to 1934, data is obtained from the National Bureau of Economic Research (NBER), as explained by Welch and Goyal (2007). Again, these rates are nominal, implying that inflation has to be taken account for.

As we subtract inflation from both market returns and risk-free rate, looking at inflation seems irrelevant. However, Bandi et al. (2019) do not use the same inflation rates for the market returns and the risk-free return. This should not be the case, as inflation is a general measure of the economy

and its price level. It seems that Bandi et al. (2019) use inflation for the risk-free rate that originates from an outdated file (the 2014 version of data from the website of Amit Goyal[3]), while the most recent version of this file (2017) contains inflation numbers that are exactly equal to those for the market returns (as obtained from the CRSP). In this paper, I neglected inflation rates in calculating excess returns, as one should use the same inflation rate for both risk-free rates of return and market returns.

[3]http://www.hec.unil.ch/agoyal/

B Classical Predictive System Aggregation

For a classical predictive system on demeaned variables, we have

$$r_{t+1} = \beta v_t + u_{t+1} \tag{22}$$

$$v_{t+1} = \rho v_t + e_{t+1} \ . \tag{23}$$

When forward aggregating returns, while backward aggregating variance over horizon h, i.e. summing up h consecutive variables, equation (33) becomes

$$\sum_{i=t+1}^{t+h} r_i = \beta \sum_{i=t+1}^{t+h} v_{i-1} + \sum_{i=t+1}^{t+h} u_i \ , \tag{24}$$

for which the variance sum can be written as

$$\sum_{i=t}^{t+h-1} v_i = \rho^{h-1} \sum_{j=t-h+1}^{t} v_j + \sum_{i=t}^{t+h-1} \sum_{k=0}^{h-2} \rho^k e_{i-k} \ , \tag{25}$$

on the condition that $h > 1$. In case $h = 1$, the system boils down to (33) and (34). Now implementing (25) into (24), taking into account that the latter terms in both equations simply are error terms, one can write

$$\sum_{i=t+1}^{t+h} r_i = \beta \rho^{h-1} \sum_{j=t-h+1}^{t} v_j + u_h \ , \tag{26}$$

with u_h the combination of all error terms for horizon h, so that the two-way aggregated regression should yield a slope equal to $\beta\rho^{h-1}$, which, when h increases, should not increase. Therefore, the classical predictive system should not be able to replicate hump-shaped behavior in its slopes. This concludes the derivation.

C Dyadic Scales

The table below gives the scales and corresponding frequencies for both yearly and monthly data.

Table 7: Frequencies for the different scales based on yearly as well as monthly data. The monthly data is used for the high-frequency analysis, whereas yearly data is employed otherwise.

Yearly		**Monthly**		
Scale j	*Frequency* (in years)	*Scale j*	*Frequency* (in months)	*Frequency* (in years)
1	1 - 2	1	1 - 2	$\frac{1}{12}$ - $\frac{1}{6}$
2	2 - 4	2	2 - 4	$\frac{1}{6}$ - $\frac{1}{3}$
3	4 - 8	3	4 - 8	$\frac{1}{3}$ - $\frac{2}{3}$
4	8 - 16	4	8 - 16	$\frac{2}{3}$ - $1\frac{1}{3}$
		5	16 - 32	$1\frac{1}{3}$ - $2\frac{2}{3}$
		6	32 - 64	$2\frac{2}{3}$ - $5\frac{1}{3}$
		7	64 - 128	$5\frac{1}{3}$ - $10\frac{2}{3}$
		8	128 - 256	$10\frac{2}{3}$ - $21\frac{1}{3}$

D Haar transformation

The formula for the Haar transformation for $J = 4$ is given by

$$\begin{pmatrix} x_t \\ x_{t-1} \\ x_{t-2} \\ x_{t-3} \\ x_{t-4} \\ x_{t-5} \\ x_{t-6} \\ x_{t-7} \\ x_{t-8} \\ x_{t-9} \\ x_{t-10} \\ x_{t-11} \\ x_{t-12} \\ x_{t-13} \\ x_{t-14} \\ x_{t-15} \end{pmatrix} = (T^{(4)})^{-1} \begin{pmatrix} \pi_t^{(4)} \\ \hat{x}_t^{(4)} \\ \hat{x}_t^{(3)} \\ \hat{x}_{t-8}^{(3)} \\ \hat{x}_t^{(2)} \\ \hat{x}_{t-4}^{(2)} \\ \hat{x}_{t-8}^{(2)} \\ \hat{x}_{t-12}^{(2)} \\ \hat{x}_t^{(1)} \\ \hat{x}_{t-2}^{(1)} \\ \hat{x}_{t-4}^{(1)} \\ \hat{x}_{t-6}^{(1)} \\ \hat{x}_{t-8}^{(1)} \\ x_t \hat{-} 10^{(1)} \\ \hat{x}_{t-12}^{(1)} \\ \hat{x}_{t-14}^{(1)} \end{pmatrix}, \tag{27}$$

where $(T^{(4)})^{-1}$ is the (16 x 16) inverse Haar matrix. This matrix can be derived using the representations in (11) and (13) and is given by

Table 8: Haar matrix $J = 4$

$\frac{1}{4}$	$\frac{1}{4}$	$\frac{1}{4}$	$\frac{1}{4}$	$\frac{1}{4}$	$\frac{1}{4}$	$\frac{1}{4}$	$\frac{1}{4}$	$\frac{1}{4}$	$\frac{1}{4}$	$\frac{1}{4}$	$\frac{1}{4}$	$\frac{1}{4}$	$\frac{1}{4}$	$\frac{1}{4}$	$\frac{1}{4}$
$\frac{1}{4}$	$\frac{1}{4}$	$\frac{1}{4}$	$\frac{1}{4}$	$\frac{1}{4}$	$\frac{1}{4}$	$\frac{1}{4}$	$\frac{1}{4}$	$-\frac{1}{4}$	$-\frac{1}{4}$	$-\frac{1}{4}$	$-\frac{1}{4}$	$-\frac{1}{4}$	$-\frac{1}{4}$	$-\frac{1}{4}$	$-\frac{1}{4}$
$\sqrt{\frac{1}{8}}$	$\sqrt{\frac{1}{8}}$	$\sqrt{\frac{1}{8}}$	$\sqrt{\frac{1}{8}}$	$-\sqrt{\frac{1}{8}}$	$-\sqrt{\frac{1}{8}}$	$-\sqrt{\frac{1}{8}}$	$-\sqrt{\frac{1}{8}}$	0	0	0	0	0	0	0	0
0	0	0	0	0	0	0	0	$\sqrt{\frac{1}{8}}$	$\sqrt{\frac{1}{8}}$	$\sqrt{\frac{1}{8}}$	$\sqrt{\frac{1}{8}}$	$-\sqrt{\frac{1}{8}}$	$-\sqrt{\frac{1}{8}}$	$-\sqrt{\frac{1}{8}}$	$-\sqrt{\frac{1}{8}}$
$\frac{1}{2}$	$\frac{1}{2}$	$-\frac{1}{2}$	$-\frac{1}{2}$	0	0	0	0	0	0	0	0	0	0	0	0
0	0	0	0	$\frac{1}{2}$	$\frac{1}{2}$	$-\frac{1}{2}$	$-\frac{1}{2}$	0	0	0	0	0	0	0	0
0	0	0	0	0	0	0	0	$\frac{1}{2}$	$\frac{1}{2}$	$-\frac{1}{2}$	$-\frac{1}{2}$	0	0	0	0
0	0	0	0	0	0	0	0	0	0	0	0	$\frac{1}{2}$	$\frac{1}{2}$	$-\frac{1}{2}$	$-\frac{1}{2}$
$\sqrt{\frac{1}{2}}$	$-\sqrt{\frac{1}{2}}$	0	0	0	0	0	0	0	0	0	0	0	0	0	0
0	0	$\sqrt{\frac{1}{2}}$	$-\sqrt{\frac{1}{2}}$	0	0	0	0	0	0	0	0	0	0	0	0
0	0	0	0	$\sqrt{\frac{1}{2}}$	$-\sqrt{\frac{1}{2}}$	0	0	0	0	0	0	0	0	0	0
0	0	0	0	0	0	$\sqrt{\frac{1}{2}}$	$-\sqrt{\frac{1}{2}}$	0	0	0	0	0	0	0	0
0	0	0	0	0	0	0	0	$\sqrt{\frac{1}{2}}$	$-\sqrt{\frac{1}{2}}$	0	0	0	0	0	0
0	0	0	0	0	0	0	0	0	0	$\sqrt{\frac{1}{2}}$	$-\sqrt{\frac{1}{2}}$	0	0	0	0
0	0	0	0	0	0	0	0	0	0	0	0	$\sqrt{\frac{1}{2}}$	$-\sqrt{\frac{1}{2}}$	0	0
0	0	0	0	0	0	0	0	0	0	0	0	0	0	$\sqrt{\frac{1}{2}}$	$-\sqrt{\frac{1}{2}}$

E Aggregated Regression Tables

The following two tables are similar to Table 1 in Section 5.1, but applied to different variance proxies. Table 9 represents the statistics for the consumption variance, while Table 10 depicts the properties for the economic policy uncertainty.

Table 9: Table containing properties for forward/backward regressions (1) of NYSE/AMEX returns on consumption variance over horizon h. Panels A1 and A2 contain slope estimates (b), Newey-West t-statistics (NW), Valkanov (2003) t-statistics and R^2's.

Panel A1: $r_{t+1,t+h} = \alpha_h + \beta_h v_{t-h+1,t} + \epsilon_{t+1,t+h}$										
h	1	2	3	4	5	6	7	8	9	10
b	1.838	2.084	0.790	-0.055	-0.038	0.462	1.798	2.705	3.087	4.061
NW	1.138	2.408	0.821	-0.075	-0.043	0.436	1.657	2.502	2.574	3.507
Valkanov	0.135	0.236	0.111	-0.009	-0.006	0.079	0.327	0.497	0.554	0.747
R^2 (%)	1.828	5.380	1.250	0.009	0.004	0.633	9.894	20.300	24.000	36.542
Panel A2: $r_{t+1,t+h} = \alpha_h + \beta_h v_{t-h+1,t} + \epsilon_{t+1,t+h}$										
h	11	12	13	14	15	16	17	18	19	20
b	4.893	5.251	5.331	4.967	4.687	4.317	3.947	3.298	2.473	1.378
NW	4.242	4.920	5.553	6.096	7.409	8.028	8.173	6.117	3.920	2.021
Valkanov	0.960	1.088	1.150	1.072	1.005	0.948	0.880	0.722	0.509	0.291
R^2 (%)	48.744	55.035	57.777	54.328	51.135	48.249	44.590	35.167	21.286	8.124

Table 10: Table containing properties for forward/backward regressions (1) of NYSE/AMEX returns on economic policy uncertainty over horizon h. Panels A1 and A2 contain slope estimates (b), Newey-West t-statistics (NW), Valkanov (2003) t-statistics and R^2's

Panel A1: $r_{t+1,t+h} = \alpha_h + \beta_h v_{t-h+1,t} + \epsilon_{t+1,t+h}$										
h	1	2	3	4	5	6	7	8	9	10
b	0.025	0.028	0.025	0.013	0.009	0.012	0.019	0.026	0.030	0.034
NW	1.913	1.930	1.434	0.951	0.628	0.891	1.480	2.322	3.167	3.906
Valkanov	0.175	0.234	0.235	0.154	0.120	0.192	0.336	0.506	0.634	0.740
R^2	3.039	5.305	5.359	2.375	1.455	3.649	10.364	20.855	29.242	36.043
Panel A2: $r_{t+1,t+h} = \alpha_h + \beta_h v_{t-h+1,t} + \epsilon_{t+1,t+h}$										
h	11	12	13	14	15	16	17	18	19	20
b	0.036	0.039	0.040	0.041	0.040	0.039	0.037	0.034	0.030	0.025
NW	4.344	4.571	4.313	4.039	3.841	3.696	3.590	3.503	3.405	3.330
Valkanov	0.849	1.007	1.095	1.159	1.177	1.236	1.211	1.112	0.925	0.765
R^2	42.643	51.095	55.318	58.121	58.887	61.282	60.319	56.214	47.093	37.852

F Simulation A

For this simulation, a classical predictive system following equations (2) - (3) is generated with parameters $\beta = 1.8$, $\rho = 0.734$, $\sigma_e = 0.0095$, $\sigma_u = 0.180$ and $\rho_{u,e} = -0.045$. These values are conform with the numbers provided in Online Supplement A of Bandi et al. (2019). Note however that the standard deviation of shocks e and u are mixed up in the subscript of Table A.1 in the Online Supplement. The shocks are generated via a bivariate normal distribution, $\rho_{u,e}$ being the correlation between both shock types. The sample size $T = 85$ is chosen to equal the number of observations in the data set for the consumption variance. After having generated returns and variances following the DGP, two-way aggregated regressions are taken out. Consequently, the corresponding behavior of the slope and coefficient of determination of these regressions is investigated and compared to the case in which $\beta = 0$ (no predictability). In doing so, σ_u changes to 0.195.

The results for both the assumptions of predictability and no predictability are presented in Table 11 and 12. Both tables resemble the values given by Bandi et al. (2019) in Online Supplement A quite neatly.

F.1 Predictability

Under the assumption of predictability ($\beta = 1.8$, see section 3.1.2), we perform 100.000 simulations, for which results are reported in Table 11.

As is visible in Table 11, slope estimates decline with the aggregation horizon. This is consistent with the theoretical implication of the slope in an aggregated classical predictive system being $\beta\rho^{h-1}$. However, the data imply slopes that first increase, reach a peak, and then decrease. In fact, this

Table 11: Distribution of slope estimates from simulating via the assumption of predictability. The table reports the mean, median, standard deviation, 5th and 95th percentile of the coefficient estimates over a horizon h, running from 1 to 20.

$\boldsymbol{\beta}$										
h	1	2	3	4	5	6	7	8	9	10
Mean	1,83	1,55	1,28	1,03	0,83	0,66	0,51	0,39	0,27	0,17
Median	1,82	1,56	1,28	1,05	0,85	0,69	0,53	0,40	0,29	0,19
St. Dev.	1,52	1,61	1,71	1,81	1,92	2,03	2,15	2,28	2,41	2,55
5th	-0,65	-1,09	-1,53	-1,95	-2,33	-2,69	-3,03	-3,34	-3,68	-3,99
95th	4,34	4,20	4,07	3,98	3,93	3,94	3,99	4,07	4,16	4,26
$\boldsymbol{\beta}$										
h	11	12	13	14	15	16	17	18	19	20
Mean	0,08	0,00	-0,08	-0,15	-0,22	-0,29	-0,35	-0,41	-0,47	-0,52
Median	0,10	0,01	-0,07	-0,15	-0,22	-0,29	-0,35	-0,41	-0,47	-0,53
St. Dev.	2,68	2,83	2,97	3,13	3,29	3,46	3,63	3,81	3,98	4,16
5th	-4,29	-4,61	-4,93	-5,23	-5,53	-5,86	-6,20	-6,53	-6,86	-7,17
95th	4,40	4,56	4,70	4,87	5,06	5,26	5,47	5,70	5,94	6,17

Table 12: Distribution of R^2 from simulating via the assumption of predictability. The table reports the mean, median, standard deviation, 5th and 95th percentile of the coefficient of determination of aggregated regressions over a horizon h, running from 1 to 20.

$\boldsymbol{R^2}$										
h	1	2	3	4	5	6	7	8	9	10
Mean	2,94	4,36	5,19	5,84	6,52	7,29	8,16	9,13	10,19	11,33
Median	1,86	2,54	2,80	3,03	3,37	3,76	4,29	4,90	5,53	6,25
St. Dev.	3,22	5,05	6,28	7,24	8,10	9,00	9,95	10,95	12,03	13,15
5th	0,02	0,02	0,03	0,03	0,03	0,03	0,04	0,04	0,05	0,06
95th	9,50	14,89	18,32	20,98	23,67	26,40	29,46	32,53	35,85	39,35
$\boldsymbol{R^2}$										
h	11	12	13	14	15	16	17	18	19	20
Mean	12,52	13,76	15,03	16,36	17,72	19,11	20,52	21,94	23,32	24,65
Median	7,04	7,95	8,88	9,91	11,05	12,26	13,56	14,94	16,36	17,70
St. Dev.	14,27	15,38	16,47	17,54	18,57	19,56	20,51	21,43	22,28	23,10
5th	0,06	0,07	0,08	0,09	0,11	0,13	0,14	0,15	0,16	0,17
95th	43,26	46,87	50,13	53,70	56,84	60,03	62,93	65,76	68,27	70,68

hump-shaped behavior in the coefficient β is only captured in 5.69% of the simulations, as can be seen in Table 18. Furthermore, from Table 12 note that the average R^2 does not exceed 25% and increases over the aggregation horizon. This is in correspondence with long-run predictive behavior in regressions (Valkanov, 2003). Still, in the empirical application, the coefficient of determination reaches over 50% and follows a hump-shaped structure. Only 3.16% of the simulations have a hump-shaped R^2 with maximum reaching over 50%. Combining the two above observations on the descriptive statistics of both β and R^2, we note that in only 0.96% of the cases both are hump-shaped while R^2 exceeds 50% at its peak. A variety of combined statistics is provided in Table 18.

Table 13: Descriptive statistics on β and R^2. The table reports the percentage of simulations for which the slope and coefficient of determination of aggregated regressions follow hump-shaped behavior and R^2 exceeds 50%. A slope or R^2 contains hump-shaped behavior when the respective variable increases monotonically over years 6-12 and decreases over years 16-20. The second column contains statistics when predictability is assumed, while the third column takes β to equal zero.

Descriptive Statistic	$\boldsymbol{\beta} = 1.8$	$\boldsymbol{\beta} = 0$
β increasing 6-12 (%)	13.18	21.25
β decreasing 16-20 (%)	38.39	32.54
β hump-shaped (%)	5.69	7.72
R^2 increasing 6-12 (%)	17.84	19.17
R^2 decreasing 16-20 (%)	18.83	19.02
R^2 hump-shaped (%)	7.03	7.46
R^2 hump-shaped & $R^2 > 50\%$ (%)	3.16	3.22
R^2 hump-shaped & $R^2 > 50\%$ & R^2_{16} - $R^2_{20} > 30\%$ (%)	1.30	1.27
R^2 and β hump-shaped (%)	2.17	2.63
R^2 and β hump-shaped & $R^2 > 50\%$ (%)	0.96	1.25
R^2 and β hump-shaped & $R^2 > 50\%$ & R^2_{16} - $R^2_{20} > 30\%$ (%)	0.44	0.58

F.2 No predictability

Under the assumption of no predictability, i.e. $\beta = 0$, we again perform 100.000 simulations for which the results are presented in a similar manner to those in the previous section.

Table 14: Distribution of slope estimates from simulating via the assumption of no predictability. The table reports the mean, median, standard deviation, 5th and 95th percentile of the coefficient estimates over a horizon h, running from 1 to 20.

$\boldsymbol{\beta}$										
h	1	2	3	4	5	6	7	8	9	10
Mean	0,02	0,03	0,03	0,04	0,04	0,05	0,06	0,06	0,07	0,08
Median	0,02	0,03	0,03	0,03	0,04	0,04	0,04	0,05	0,07	0,07
St. Dev.	1,65	1,75	1,86	1,96	2,07	2,18	2,30	2,43	2,56	2,69
5th	-2,66	-2,82	-3,00	-3,17	-3,35	-3,51	-3,68	-3,86	-4,06	-4,29
95th	2,75	2,91	3,08	3,26	3,45	3,63	3,83	4,05	4,26	4,49
$\boldsymbol{\beta}$										
h	11	12	13	14	15	16	17	18	19	20
Mean	0,09	0,10	0,10	0,11	0,11	0,11	0,11	0,12	0,12	0,13
Median	0,08	0,09	0,10	0,10	0,11	0,11	0,11	0,11	0,12	0,14
St. Dev.	2,84	2,99	3,15	3,32	3,49	3,67	3,85	4,04	4,23	4,41
5th	-4,50	-4,72	-4,98	-5,22	-5,48	-5,76	-6,05	-6,37	-6,65	-6,94
95th	4,72	4,94	5,19	5,48	5,73	6,03	6,31	6,61	6,92	7,19

From Table 14, we see an increasing mean β estimate over horizon h. A similar pattern is visible for the coefficients of determination, see Table 15. This is in correspondence with so-called unit root behavior. Due to simply summing up observations, dependence between consecutive points arises while shocks have longer-lasting effects. Still, the behavior of both β and R^2 does not seem to match the behavior found in the data. To illustrate this, again, a variety of descriptive statistics is reported in Table 18. It is apparent that these statistics do not deviate all too much from those

under the assumption of predictability. For instance, the percentage of simulations for which both β and R^2 are hump-shaped while R^2 exceeds 50% in its peak is only 1.25%. In similar fashion as in the previous section, we can thus state that assuming *no* predictability in returns does not allow us to replicate the hump-shaped behavior in the data.

Table 15: Distribution of R^2 from simulating via the assumption of no predictability. The table reports the mean, median, standard deviation, 5th and 95th percentile of the coefficient estimates over a horizon h, running from 1 to 20.

R^2										
h	1	2	3	4	5	6	7	8	9	10
Mean	1,20	2,28	3,36	4,44	5,53	6,63	7,76	8,92	10,12	11,34
Median	0,56	1,08	1,62	2,18	2,76	3,38	4,04	4,76	5,52	6,35
St. Dev.	1,67	3,09	4,47	5,79	7,09	8,33	9,53	10,71	11,90	13,06
5th	0,00	0,01	0,01	0,02	0,02	0,03	0,04	0,04	0,05	0,06
95th	4,57	8,64	12,65	16,51	20,59	24,36	28,16	31,93	35,64	39,41
R^2										
h	11	12	13	14	15	16	17	18	19	20
Mean	12,59	13,86	15,16	16,49	17,82	19,16	20,53	21,90	23,23	24,51
Median	7,19	8,11	9,07	10,05	11,13	12,24	13,49	14,75	16,10	17,51
St. Dev.	14,22	15,36	16,48	17,59	18,64	19,64	20,59	21,48	22,29	23,03
5th	0,07	0,07	0,08	0,09	0,10	0,12	0,13	0,14	0,16	0,17
95th	43,03	46,73	50,45	53,82	56,99	60,16	63,16	65,98	68,31	70,46

G Multiple Regressor System

Table 16 reports R^2-values, coefficient estimates and t-statistics in scale-specific predictive regressions with the five predictors; market variance, consumption variance, economic policy uncertainty, dividend yield and inflation. The table is based on the NYSE/AMEX index.

Table 16: Coefficient estimates, t-statistics and R^2 of predictive regressions of excess market returns on market variance, consumption variance, EPU, dividend yield and inflation, based on the NYSE/AMEX index, so that $M = 5$ equals the number of predictors.

$\mathrm{r}_{t+2^j}^{(j)} = \beta_{1,j} x_{1,t}^{(j)} + \beta_{2,j} x_{2,t}^{(j)} + ... + \beta_{M,j} x_{M,t}^{(j)} + u_{t+2^j}^{(j)}$								
Scale j	1		2		3		4	
Predictor m	$\hat{\beta}_{m,j}$	*t-stat*	$\hat{\beta}_{m,j}$	*t-stat*	$\hat{\beta}_{m,j}$	*t-stat*	$\hat{\beta}_{m,j}$	*t-stat*
Market Variance	1.01	(0.97)	-0.42	(-0.50)	0.26	(0.39)	-1.25	(-1.06)
Consumption Variance	5.67	(1.99)	-4.59	(-2.24)	-0.54	(-0.39)	4.95	(2.32)
EPU	-0.01	(-0.45)	0.01	(0.36)	-0.01	(-0.53)	0.03	(2.39)
Dividend Yield	0.32	(1.45)	-0.24	(-1.20)	0.44	(2.78)	-0.04	(-0.18)
Inflation	0.26	(0.29)	0.24	(0.37)	1.27	(2.82)	0.36	(0.99)
R^2 (%)	8.80		9.05		27.51		42.35	

H Simulation B

The second simulation constitutes generating data following the system (14) - (15). In doing so, it is assumed that predictability is only existent for cycles between 8 and 16 years (j = 4), with $\beta_4 = 2.80$ and all other $\beta's$ zero. The autoregressive parameter ρ_4 is set equal to 0.2, while all other $\rho's$ are set to 0. The shocks $u^{(4)}_{k2^4+2^4}$ are also set to zero to make sure hump-shaped behavior is not a result of spurious behavior. As for the shocks u and e, correlation between the two different shock series is assumed to be zero. The variance parameters $\sigma^{(j)}_u$ are computed from the data and given by 0.02, 0.012 and 0.005 for j = 1,2,3. The variance parameters $\sigma^{(j)}_e$ are given by the authors to be 0.257, 0.354, 0.437 and 0.377 for j = 1,2,3,4. To investigate hump-shaped behavior in aggregated models, the generated observations should be transformed from scale time into calendar time. This transformation can be taken out by multiplying the inverse Haar matrix with a column vector of scale-time data, see Appendix D. Simulation B also contains contemporaneous aggregation, i.e. forward/forward aggregation of excess market returns and market variance, to confirm that predictability in forward/backward aggregation is not coincidental. The assumption of no predictability is simulated as well, which results in

$$r^{(j)}_{k2^j+2^j} = u^{(j)}_{k2^j+2^j} \quad j = 1, ..., 4 \ , \tag{28}$$

so that the slope β equals zero.

All simulations in this sections have sample size $T = 128$ and 10.000 replications.

H.1 Predictability

Under the assumption of predictability, where we take β_4 in (14) to equal 2.8 in correspondence with Bandi et al. (2019), the results for performing forward-backward regressions are provided in Table 17. Both the median of β and of R^2 seem to follow hump-shaped behavior, in the sense that both increase until reaching a peak at $h = 16$, after which both decrease again. The peak for the R^2 takes on a median value of 47.41%. However, it is striking that the median adjusted R^2 is negative for a horizon of 1, which should not happen. Furthermore, the coefficient of determination seems to increase until $h = 7$, after which a decrease kicks in until the aggregation horizon exceeds 10. This 'double hump-shaped behavior' distorts the results when evaluating this simulation on the same basis as Table 8. Therefore, we consider the R^2 to possess hump-shaped behavior when it increases from $h = 9$ until $h = 13$, while decreasing from a horizon of 16 to 20 years. Descriptive statistics

are provided in Table 18, column 1.

Table 17: Statistics for the simulation of scale-specific systems based on the assumption of predictability for the fourth scale. For a horizon h of 1 to 20, the table reports the median and standard deviation of the slope and median of the adjusted coefficient of determination for forward-backward aggregated regressions.

A1										
h	1	2	3	4	5	6	7	8	9	10
Median β	0,02	-0,01	-0,07	-0,19	-0,36	-0,51	-0,57	-0,51	-0,29	0,03
St. Dev. β	0,11	0,16	0,22	0,26	0,30	0,32	0,34	0,35	0,36	0,38
Median Adj. R^2	-0,31	0,04	0,62	1,86	5,20	9,03	10,46	7,48	2,15	0,94
A2										
h	11	12	13	14	15	16	17	18	19	20
Median β	0,38	0,72	0,96	1,14	1,26	1,31	1,28	1,21	1,11	0,95
St. Dev. β	0,39	0,42	0,46	0,51	0,54	0,56	0,55	0,52	0,49	0,48
Median Adj. R^2	3,78	13,67	25,75	36,97	44,67	47,41	45,42	40,37	32,84	23,83

Table 18: Distribution of slope estimates from simulating via the assumption of predictability (2nd column, forward-backward), no predictability (3rd column) and contemporaneous regressions (4th column, forward-forward). The table reports the mean, median, standard deviation, 5th and 95th percentile of the coefficient estimates over a horizon h, running from 1 to 20.

Descriptive Statistic	$\boldsymbol{\beta_4, fb} = 2.8$	$\boldsymbol{\beta_4} = 0$	$\boldsymbol{\beta_4, ff} = 2.8$
β increasing 6-12 (%)	30.69	5.24	1.43
β decreasing 16-20 (%)	52.48	11.56	3.48
β hump-shaped (%)	21.43	1.36	0.29
R^2 increasing 9-13 (%)	33.86	8.82	50.17
R^2 decreasing 16-20 (%)	58.24	9.24	43.52
R^2 hump-shaped (%)	28.38	2.12	32.01
R^2 hump-shaped & $R^2 > 50\%$ (%)	19.24	0.04	1.08
R^2 hump-shaped & $R^2 > 50\%$ & R^2_{16} - $R^2_{20} > 30\%$ (%)	14.80	0.01	0.07
R^2 and β hump-shaped (%)	17.59	0.43	0.06
R^2 and β hump-shaped & $R^2 > 50\%$ (%)	13.28	0.01	0.00
R^2 and β hump-shaped & $R^2 > 50\%$ & R^2_{16} - $R^2_{20} > 30\%$ (%)	10.84	0.00	0.00

H.2 No predictability

Similar to the assumption of predictability, taking β_j to be zero for all j = 1,2,3,4 can be investigated as well. This is done as to find out whether the possible hump-shaped behavior is actually due to assuming predictability. The results for forward-backward aggregated regressions are given in Table19.

From this table, we can see that the median slope estimates approximate zero for all aggregation horizons, which is conform the data generating process. Furthermore, the R^2 again is negative at the beginning (small h), while its magnitude remains small over all horizons. The third column of Table 18 reports descriptive statistics for the assumption of no predictability. From these statistics it can be seen that the likeliness of hump-shaped behavior is much smaller than for the assumption of

Table 19: Statistics for the simulation of scale-specific systems based on the assumption of no predictability for the fourth scale. For a horizon h of 1 to 20, the table reports the median and standard deviation of the slope and median of the adjusted coefficient of determination for forward-backward aggregated regressions.

B1										
h	1	2	3	4	5	6	7	8	9	10
Median β	0,00	0,00	0,00	0,00	0,00	0,00	0,00	0,00	0,00	0,00
St. Dev. β	0,02	0,02	0,02	0,02	0,02	0,02	0,02	0,02	0,02	0,02
Median Adj. R^2	-0,40	-0,31	-0,16	-0,03	0,15	0,26	0,41	0,38	0,44	0,51
B2										
h	11	12	13	14	15	16	17	18	19	20
Median β	0,00	0,00	0,00	0,00	0,00	0,00	0,00	0,00	0,00	0,00
St. Dev. β	0,02	0,03	0,03	0,03	0,03	0,03	0,03	0,03	0,03	0,03
Median Adj. R^2	0,62	0,69	0,76	0,90	1,15	1,30	1,22	1,03	0,95	0,92

predictability. The percentage of simulations for which both β and R^2 show hump-shaped behavior lies around 0.43%, while imposing the restriction of R^2 exceeding 50% leaves us with only 0.01% of the simulations.

H.3 Contemporaneous Aggregation

In correspondence with Online Supplement B of Bandi et al. (2019), we investigate whether forward/-forward aggregation of returns and variance may yield (hump-shaped behavior in) predictability. The results from such aggregated regressions are provided in Table 20.

Table 20: Statistics for the simulation of scale-specific systems based on the assumption of predictability for the fourth scale. For a horizon h of 1 to 20, the table reports the median and standard deviation of the slope and median of the adjusted coefficient of determination for forward-forward aggregated regressions.

C1										
h	1	2	3	4	5	6	7	8	9	10
Median β	0,03	0,05	0,06	0,07	0,07	0,07	0,05	0,03	-0,02	-0,08
St. Dev. β	0,08	0,14	0,20	0,25	0,30	0,35	0,39	0,42	0,44	0,46
Median Adj. R^2	-0,33	0,03	0,40	0,79	1,19	1,48	1,74	1,99	2,28	2,58
C2										
h	11	12	13	14	15	16	17	18	19	20
Median β	-0,15	-0,23	-0,30	-0,37	-0,42	-0,45	-0,43	-0,38	-0,32	-0,24
St. Dev. β	0,47	0,47	0,47	0,47	0,47	0,47	0,47	0,47	0,48	0,49
Median Adj. R^2	2,92	3,31	4,05	5,04	5,92	6,56	5,97	4,92	4,10	3,39

As Table 20 illustrates, hump-shaped behavior of the slope of forward-forward aggregated regressions does not seem to be apparent. In fact, the median slope is lowest for an aggregation horizon of 16 years. As for the adjusted coefficient of determination, its magnitude is relatively small throughout all values of h, although there seems to be some kind of upward trend until $h = 16$, after which the R^2 decreases again. Still, Table 20 does not seem able to capture the empirical hump-shaped behavior. This is again illustrated by Table18, in which a variety of descriptive statistics is given.

From these statistics, it can be deducted that a hump-shaped R^2 is present in 32.01% of all simulations, which is a substantial part. However, due to the small magnitude of these R^2's, as well as hardly any hump-shaped β, the percentage of simulations for which both the slope and coefficient of determination are hump-shaped while the peak of the R^2 exceeds 50% is equal to 0.00%. This confirms the hypothesis of contemporaneous aggregation not being able to replicate the behavior observed in the data.

I Note

This research has adjusted data compared to the data used by Bandi et al. (2019), based on the belief that slight mistakes were made. Therefore, the results presented in Section 5.1 are not completely equal to those presented by Bandi et al. (2019). However, I have been able to exactly replications these results. Results are available upon request or can be generated using the code in Appendix K. As a practical sidenote, it should be said that Bandi et al. (2019) use the sample period 1933 to 2014 for market variance, 1931 to 2014 for consumption variance, and 1930 to 2014 for economic policy uncertainty.

J Monthly returns derivation

The monthly CRSP return data including dividends, VWRETD, and the data excluding dividends, VWRETX, are used as a starting point, while the price index at $t = 0$ is set equal to 100. The monthly simple returns including dividends are calculated by using

$$r_t = \frac{D_t + P_t}{P_{t-1}} - 1 \qquad t = 1, ..., T \ , \tag{29}$$

with D_t and P_t noting dividends and the price index at time t respectively. The price index at time t is rewritten as

$$P_t = P_{t-1}(1 + VWRETX_t) \qquad t = 1, ..., T \ , \tag{30}$$

while the dividends at time t are denoted by

$$D_t = P_t(\frac{VWRETD_t + 1}{VWRETX_t + 1} - 1) \qquad t = 1, ..., T \tag{31}$$

The above is exactly what Bandi et al. (2019) do to find monthly simple returns including dividends. However, it can be shown that, using the above equations, r_t should exactly equal $VWRETD_t$. Namely,

$$\begin{aligned}
r_t &= \frac{D_t + P_t}{P_{t-1}} - 1 \\
&= \frac{P_t(\frac{VWRETD_t+1}{VWRETX_t+1} - 1) + P_{t-1}(1 + VWRETX_t)}{P_{t-1}} - 1 \\
&= \frac{P_{t-1}(1 + VWRETX_t)(\frac{VWRETD_t+1}{VWRETX_t+1} - 1) + P_{t-1}(1 + VWRETX_t)}{P_{t-1}} - 1 \\
&= \frac{P_{t-1}(1 + VWRETD_t) - P_{t-1}(1 + VWRETX_t) + P_{t-1}(1 + VWRETX_t)}{P_{t-1}} - 1 \\
&= \frac{P_{t-1}(VWRETD_t + 1)}{P_{t-1}} - 1 \\
&= VWRETD_t
\end{aligned} \tag{32}$$

This concludes the derivation that monthly CRSP returns should equal monthly returns formed via the transformation of Bandi et al. (2019).

K Codes

In this appendix, I will briefly explain the codes used. With this paper, I send a ZIP-file with all codes (including a .txt-file containing explanations). However, I will give a short explanation to every code here.

K.1 Folder Annual Analysis

consumptionvar.m: generates a vector with consumption variance observations over the sample period.

corrscale.m: computes correlations between the redundant data across different scales.

dividendyield.m: generates a vector of dividend yields for either the NYSE/AMEX or S&P 500 index.

epu.m: generates a vector of EPU variance observations over the sample period.

excessreturns.m: generates a vector of excess returns from either the NYSE/AMEX or S&P 500 index.

laglength.m: generates a matrix containing the R^2's for all combinations of aggregation horizons between regressand and regressor.

Main.m: the code that links all other codes together and reports all results when run. This is the code of main interest.

marketvar.m: generates a vector of market variance observations from either the NYSE/AMEX or S&P 500 index.

MultipleMain.m: the code that links all other codes together for the multiple regressor extension. This code should be run to retrieve all results in Section 5.2.3.

multipolsaggregate.m: code that runs two-way aggregated regressions for a system with multiple regressors.

multipredreg.m: code that runs scale-specific predictive regressions for a system with multiple regressors.

normtoscale.m: code that transforms regular time series observations into (redundant) scale-specific points.

nwest.m: not my own code, but retrieved online; runs a Newey-West regression.

olsaggregate.m: code that runs two-way aggregated regressions for a system with a single regressor.

predreg.m: code that runs scale-specific predictive regressions in a system with a single regressor.

scalehorizon.m: code that returns properties of scale-specific regressions for all possible combinations of scales for regressand and regressor.

scaletodec: code that transforms scale-specific calendar-time observations to decimated points.

T4inv.m: code that returns the Haar and inverse Haar matrix for $J = 4$.

K.2 Folder High-frequency Extension

corrscale.m: computes correlations between the redundant data across different scales.

excessreturns.m: generates a vector of excess returns from either the NYSE/AMEX or S&P 500 index, based on monthly observations.

Main.m: the code that links all other codes together and reports all results when run. This is the code of main interest.

marketvar.m: generates a vector of market variance observations from either the NYSE/AMEX or S&P 500 index.

normtoscale.m: code that transforms regular time series observations into (redundant) scale-specific points.

nwest.m: not my own code, but retrieved online; runs a Newey-West regression.

olsaggregate.m: code that runs two-way aggregated regressions for a system with a single regressor.

predreg.m: code that runs scale-specific predictive regressions in a system with a single regressor.

predregFTSEAEX.m: code that runs scale-specific predictive regressions for either the FTSE 100 or AEX index.

scaletocec.m: code that transforms scale-specific calendar-time observations to decimated points.

T4inv.m: code that returns the Haar and inverse Haar matrix for $J = 4$.

K.3 Folder Simulations

simulationA.m: runs the first simulation (based on classical predictive systems).

SimulationB.m: runs the second simulation (based on scale-specific classical predictive systems).

K.4 Folder Exact Replication Codes

consumptionvar.m: generates a vector with consumption variance observations over the sample period.

corrscale.m: computes correlations between the redundant data across different scales.

epu.m: generates a vector of EPU variance observations over the sample period.

excessreturns.m: generates a vector of excess returns from the NYSE/AMEX index.

Main.m: the code that links all other codes together and reports all results when run. This is the code of main interest.

marketvar.m: generates a vector of market variance observations from the NYSE/AMEX index.

normtoscale.m: code that transforms regular time series observations into (redundant) scale-specific points.

nwest.m: not my own code, but retrieved online; runs a Newey-West regression.

olsaggregate.m: code that runs two-way aggregated regressions for a system with a single regressor.

predreg.m: code that runs scale-specific predictive regressions in a system with a single regressor.

scaletocec.m: code that transforms scale-specific calendar-time observations to decimated points.

T4inv.m: code that returns the Haar and inverse Haar matrix for $J = 4$.